# CORROSION FATIGUE STUDIES ON A NUCLEAR PRESSURE VESSEL STEEL IN SIMULATED PRESSURIZED WATER REACTOR ENVIRONMENTS

P.D. HICKS

# Corrosion Fatigue Studies on a Nuclear Pressure Vessel Steel in Simulated Pressurized Water Reactor Environments

Peter David Hicks

A Dissertation Submitted to the Faculty of Engineering, University of the Witwatersrand, Johannesburg, for the Degree of Master of Science in Engineering

Department of Metallurgy
University of the Witwatersrand
Johannesburg

January 1985

## SYNOPSIS

This project involves the initial stages of the setting up of a high temperature high pressure rig to undertake corrosion fatigue tests in a simulated pressurized water reactor (P.W.R.) environment. The project included:

a) Setting up of a water purification and dosing unit to simulate P.W.R. water chemistries.

b) Rig design for low temperature (20 - 95 °C) low pressure (up to $^1/_2$ atm $H_2$ over pressure) corrosion fatigue testing in P.W.R. environments.

c) Rigorous mechanical and microstructural evaluation of a section of SA508 C.3 forged steel nuclear reactor nozzle.

d) Corrosion fatigue tests to check the effects of testing temperature (20 and 50 °C), sample orientation to the main forging, R-ratio (0.7 and 0.2), frequency (1 and 10 Hz) and environment (air. vs. P.W.R. tests). The corrosion fatigue test specimens were examined under the S.E.M. to establish the fractographic features.

e) Sample potential monitoring during corrosion fatigue testing, and related potentiodynamic work.

The project has led to several important conclusions:

1) Sulphide inclusion (MnS) clusters increase crack growth rates and they contribute to enhanced corrosion fatigue crack growth rates by acting as hydrogen trap sites.

2) Sample potential monitoring and potentiodynamic studies showed that specimen isolation from the clevis is not required. Use

of the Pourbaix diagram in the Fe-$H_2O$ system shows that the pressure vessel material lies in the corrosion régime.

3) Anodic dissolution and hydrogen embrittlement mechanisms have been proposed for the environmental enhancement of crack growth rates. However, regions of fast crack growth (observed fractographically) about MnS inclusions can be more easily explained by the hydrogen embrittlement mechanism.

4) Compact tension (C.T.) specimens orientated parallel to the MnS stringer inclusions give high crack growth rates. For increases in temperature and decreases in frequency, crack growth rates are higher than corresponding low temperature, high frequency tests. Clearly the role of MnS inclusions cannot be ignored (the MnS inclusions were found to be inclined at an angle to the inside nozzle surface).

5) The 0.7 R-ratio and the orientation air tests resulted in crack growth rates greater than those predicted by the A.S.M.E. XI 1980 air line data. Clearly more rigorous codes are required for this type of testing.

Clearly, such a test facility will lead to the production of 'useful' (meaningful) results. It is hoped that active involvement in the affairs of the International Cyclic Crack Growth Rate group (I.C.C.G.R.) will lead ultimately to the University of the Witwatersrand gaining fellowship with the group.

## DECLARATION

I, Peter David Hicks, declare that this dissertation is my own work. It is being submitted for the degree of Master of Science in Engineering at the University of the Witwatersrand, Johannesburg. It has not been submitted before for any degree or examination at any other University.

10th day of January, 1985.

**ACKNOWLEDGEMENTS**

The author would like to acknowledge the co-operation and assistance given by the following persons and organizations:

Professor F P A Robinson
his supervisor for his guidance and interest throughout the duration of the project,

Dr J Bulloch
his co-supervisor for his assistance, experience and useful suggestions,

Professor G G Garrett
for initiating an overseas visit to the I.C.C.G.R. Conference and for his interest and assistance,

Mr R B Tait
for his interest and assistance,

Mr R Achilles
for his assistance with certain experimental details,

The Atomic Energy Commission
for their substantial financial support. Dr K Bogie for his assistance. Mr D de G Jones for his useful suggestions and discussions, and the library staff for their reliable literature searching facilities.

The C.S.I.R.
his employers (Dr J B Clark and Dr N R Comins) for their co-operation.

The typist (Adele Forman)
for her patience and typing skills.

His mother (Mrs P M Hicks)
for her proof-reading capabilities.

## CONTENTS

## 1 0 INTRODUCTION

Large steel fabrications have been used in the nuclear power industry as the pressure vessel to enclose the reactor primary system. The light water cooled and moderated power reactors contain high temperature potentially radioactive deionized water, circulating through the primary system. This is a light corrosive environment as regards the structural component materials. The properties (intergranular stress corrosion, corrosion fatigue, etc.) have been localized phenomena, exacerbated in general by the fact that the environment is not highly corrosive.

Recently some unfortunate cases of failure have been experienced in weld overlay liners. For example, the Japanese Power Demonstration Reactor, was found to contain cracks in the overlay, and some of those in the top head wall penetrated through the liner to the base metal. This led to the necessity to evaluate the effect of crack propagation in the low alloy steel vessel. Despite the abundance of engineering test data, the basic nature of the corrosion of steels in such an environment has not as yet been amply clarified.

In view of the importance of this aspect of corrosion fatigue an international body was established to consider the problem. The formation took place in the late seventies and has evolved to become known as the I.C.C.G.R. group (International Cyclic Crack Growth Rate). It consisted initially of U.S.A. companies, General Electric and Westinghouse with French (C.E.A/Framatone) and British (U.K.A.E.A.) contingents. The object of this scientific body was collaborative research into the various aspects of corrosion fatigue of SA 533 Grade B and SA 508 Class 3 steels, under simulated reactor conditions. In particular it was intended to identify those parameters having an influence on corrosion fatigue crack propagation. Typical parameters included are: temperature, pressure, electrochemistry, impurities in the steel (especially sulphur and phosphorous), oxygen content of the environment, water conductivity, its impurity content and composition, waveform, frequency, fatigue force ratio R, stress level, transient history, flowrate, strain rate, incubation time, increasing/decreasing $\Delta K$, constant $\Delta K$,

and several others. Ultimately the group aims to set up international specifications and standards for such reactor pressure vessels for long term integrity and safety considerations.

The most important aim of this project is therefore to provide meaningful results to contribute to the development of calculations for nuclear pressure vessel safety requirements. Also, for the benefit of South Africa (A.E.C. and the University of the Witwatersrand) it is essential that original, useful results are generated in this field to facilitate membership of the I.C.C.G.R. group. Active participation in I.C.C.G.R. conferences will be required so that other countries can benefit from our research and vice versa. Clearly such interaction will lead to a better understanding (world-wide) of corrosion fatigue within nuclear pressure vessels.

To fulfil the above objectives, corrosion fatigue testing in the Department of Metallurgy will need to be carried out in truly representative P.W.R. environments. This project represents the first stage of a test programme which will initially involve the design of a low temperature and low pressure loop to simulate P.W.R. conditions within a test cell. Tests will then be carried out to check the effect of water temperature, sample orientation with respect to the forged pressure vessel material, frequency of fatigue, R-ratio ($K_{min}/K_{max}$) and waveform of loading cycle. Random sample potential measurements will be carried out on some of the samples in the test programme.

The water purification and control loop will ultimately serve the high temperature, high pressure corrosion fatigue loop that is to be built. Active experimentation in this field is required to achieve fellowship of the I.C.C.G.R. group.

## 2.0 LITERATURE SURVEY

### 2.1 AQUEOUS CORROSION FATIGUE

Corrosion fatigue in metals may be defined as the synergistic or combined action of an aggressive environment and a cyclic stress leading to premature failure by cracking. The majority of observed fatigue failures are, in fact, corrosion fatigue failures, since only fatigue occurring in an absolute vacuum could be termed as pure 'fatigue'.

Corrosion fatigue should not be confused with stress corrosion cracking. All metals which are susceptible to corrosion are liable to undergo corrosion fatigue damage. Generally speaking, stress corrosion cracking is suffered by alloys in very specific environments (i.e. the 'specific ion' effect), and is normally investigated under conditions of static tensile rather than of dynamic stress.

The major effect of corrosion on the form of the S-N curve is that fatigue limits in the true sense are removed. Therefore, a finite lifetime at any tensile stress or stress amplitude tends to exist, provided that cyclic loading is continued for sufficiently long periods in the environment. It is worth noting that fatigue life is often prolonged at high stress amplitudes by the presence of certain environments, so that corrosion may lead to an S-N curve of the form of either A or B in Fig. 2.1.

According to Gilbert [1]:

1. Corrosion fatigue cracks are usually transcrystalline, although there have been examples of intercrystalline failure.

2. Corrosion fatigue often produces branched cracks rather than the single fronted crack characteristic of fatigue in air.

3. Corrosion fatigue, under total immersion conditions is an electrochemical phenomenon, because it can be prevented by cathodic protection or by the addition of inhibitors to the corroding solution.

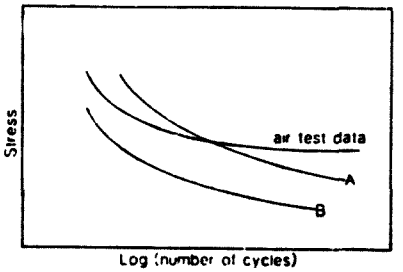


FIGURE 2.1: Schematic S-N curves for air and corrosion fatigue tests, A-corrosion fatigue showing retarded initiation at high stress, B-corrosion fatigue giving a general lowering of fatigue strength.

4. The corrosion fatigue limit, assessed usually as a stress that gives failure in a specific lifetime, is insensitive to metallurgical conditions and shows little correlation with strength, in contrast to the relatively good correlation between the tensile strength and air fatigue strength of many alloys [2, 3].

## 2 1.1 The Application of Fracture Mechanics to Corrosion Fatigue studies

The tensile stress ahead of a sharp crack is given by Westergaard [4] as:

$$\sigma_{yy} = \frac{K}{(2\pi r)^{1/2}} \qquad (2.1)$$

where $\sigma_{yy}$ is the stress normal to the plane of the crack and r the distance measured from the crack tip. Thus, the stress field just ahead of a sharp crack can be characterized by K (stress intensity factor) under linear elastic conditions and appropriate corrections can be made for finite sized specimens and various

crack geometries. If the crack faces are displaced normal to the crack plane during fracture the relevant stress intensity is designated $K_I$ (opening mode I cracking) and an additional subscript c is used to denote the critical K level (say for unstable crack propagation) Hence, provided that certain test geometry restrictions are conformed to a material parameter, $K_{Ic}$, can be evaluated experimentally to describe the toughness of precracked material under linear elastic (plain strain) conditions.

There has been a significant move in recent years towards the collection of fatigue data using the fracture mechanics approach because in principle the data can be made specimen independent in the sense that tests on different geometry specimens of the same material should produce the same crack growth versus stress intensity data. The actual parameters of importance in corrosion fatigue data collection are $K_{min}$, $K_{max}$, the minimum and maximum values of K in a load cycle, and $\Delta K = (K_{max} - K_{min})$. These are functions of crack length as well as load so they may or may not vary throughout the test, depending upon the details of the specimen type and the loading schedule. Additionally, the mean stress may also be important. This is normally expressed in terms of the fatigue force ratio or R ratio, where $R = \sigma_{min}/\sigma_{max}$. Hence, R is positive for tension-tension tests, zero for reversed bending with a minimum stress of zero and negative for compression-tension tests.

As $K = \Pi^{1/2}\ \sigma_{app}\ a^{1/2}$ f(specimen size, crack size, yield strength) it is clear that:

$$1 - R = 1 - \sigma_{min}/\sigma_{max} = \Delta K/K_{max} \qquad (2.2)$$

Thus R, $\Delta K$ and $K_{max}$ are not independent test variables and care is necessary when interpreting data where all of these parameters are apparently varied, or in comparing data plotted with different co-ordinate axes.

Another point of some significance for corrosion fatigue testing is the phenomenon of crack closure as described by Elber [5]. Briefly in an elastic-plastic medium that undergoes limited plastic defor-

mation at the crack tip during loading, it is possible for the crack faces to impinge during unloading before the tensile load is completely removed. For thin plates, Elber suggested that this reduced the effective $\Delta K$ during fatigue and has proposed the empirical relationship

$$\Delta K_{effective} = (0.5 + 0.4\ R)\ \Delta K_{apparent} \qquad (2.3)$$

based on the results of tests on aluminium. However, crack closure effects are yet far from being fully understood. This is not surprising because the details of what conditions pertain to a deforming crack tip in a corrosive environment are extremely difficult to investigate.

In any crack growth situation, the most dominant cracking mechanism is likely to control the growth rate. Thus, for high frequency loading, air fatigue growth rates tend to be unaltered by the presence of an aqueous corrosive environment simply because there is insufficient time per cycle for corrosive effects to influence significantly fatigue crack growth. For many systems, air fatigue crack growth occurs only above a threshold stress intensity factor amplitude, $\Delta K_{th}$. The growth per cycle first increases rapidly with increasing $\Delta K$ above $\Delta K_{th}$ then enters a region where log da/dN is linearly dependent upon log $\Delta K$ and finally becomes very rapid as $K_{max}$ approaches $K_c$ or $K_{Ic}$. This is shown schematically in Fig. 2.2a. In contrast, for many systems that stress-corrode, there is a definable stress intensity factor below which crack growth will not occur, termed $K_{ISCC}$, and the log (crack growth rate) versus log K curve first rises steeply and frequently reaches a plateau value that is independent of K, then rises steeply again when K approaches $K_c$ or $K_{Ic}$ as indicated in Fig. 2.2b.

There are thus three possible forms for log da/dN versus log $\Delta K$ environment-assisted fatigue curves, as shown in Figs 2.2c, d and e. The shape of curve depends on whether or not there is a synergistic effect of the corrosive environment and the alternating stress that is independent of any stress corrosion mechanism. It also depends

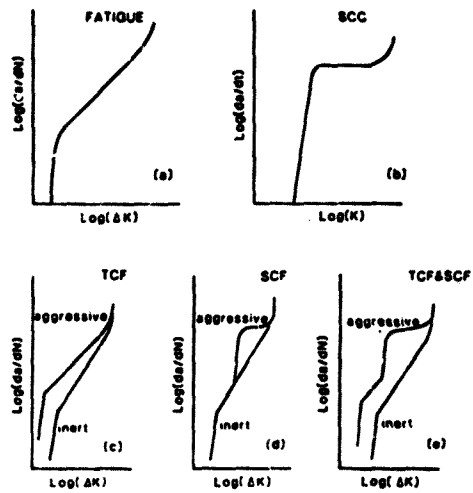


FIGURE 2.2: Schematic illustrations of basic types of corrosion fatigue behaviour. SCC = stress corrosion cracking; TCF = true corrosion fatigue; SCF = stress corrosion fatigue [58].

on what value the minimum stress intensity for stress corrosion ($K_{ISCC}$) if it exists, has in relation to $\Delta K_{th}$. Now the contribution to crack growth from stress corrosion depends upon $K_{max}$, whereas $\Delta K$ is the controlling parameter for fatigue crack growth. Since $\Delta K/K_{max} = 1 - R$ it is not surprising that much corrosion fatigue data shows an R dependence, whereas air fatigue results are generally independent of R value.

Paris and Erdogan [6] suggested that at least part of the fatigue crack growth conformed to the relationship:

$$da/dN = C\,\Delta K^{n} \qquad (2.4)$$

The exponent n varies considerably and there is a systematic variation of C with n. The Paris equation is only valid for the intermediate $\Delta K$ range where the log da/dN versus log $\Delta K$ plot is linear. This range is a useful region to consider for investigations into the mechanism of corrosion fatigue because it is reasonably certain that in this range, growth by both air and corrosion fatigue is often by a ductile striation mechanism.

As previously described in relation to Fig. 2.2 c, d and e there are three types of log da/dN versus log $\Delta K$ plot that may result when a material is fatigue loaded in the presence of an aqueous environment. Figure 2.2(c) is typical of the behaviour exhibited by systems for which stress corrosion cracking does not occur under static loads and has been termed 'true corrosion fatigue' [11]. As can be seen, the environmental fatigue curve exhibits different values of C and n in the Paris equation from those relevant to an inert environment. In contrast Figs 2.2 d and e show behaviour typical of systems which exhibit stress corrosion cracking under static loads when the maximum stress intensity exceeds a threshold value designated $K_{ISCC}$. For the system shown in Fig. 2.2(d), environmental enhancement of cyclic growth rates is only exhibited when the stress intensity range $\Delta K$ is such that the maximum stress intensity attained during the fatigue cycle exceeds $K_{ISCC}$. This has been termed stress corrosion fatigue. For the system shown in Fig. 2.2(e), stress corrosion fatigue appears to be superimposed on the corrosion fatigue so that environmental enhancement of cyclic crack growth rates is also exhibited when $K_{max} < K_{ISCC}$. The latter type of behaviour is the most common type of behaviour shown by material/environment systems exhibiting so-called 'stress corrosion fatigue'.

It is clear that any detailed mechanism of environmental crack growth must be able to explain all the experimental facts particularly in relation to the effects of cyclic frequency, loading wave form, mean stress (i.e. stress ratio), applied potential and the pH of the environment (especially near the crack tip). Whilst it is primarily the potential of the metal and the pH of the environment

within the crack enclave that will determine which of the various electrochemical reactions are possible at the crack tip, mechanical variables such as frequency, wave form and mean stress may influence reaction kinetics and in so doing determine which reactions actually occur at the crack tip.

### 2.1.2 Models and Mechanisms for Corrosion Fatigue Crack Propagation

The mechanisms that have been proposed to account for enhanced crack growth resulting from the presence of a corrosive environment during cyclic loading are not essentially different from those invoked in explaining stress corrosion cracking. Thus it has been suggested [8] that localized plastic deformation arising from cyclic loading causes the disruption of otherwise protective surface films and hence promotes electrochemical activity. This sustains selective corrosion related to an inherent tendency to intergranular corrosion and also facilitates the ingress of hydrogen into a metal to promote crack growth. This effect can even lower the energy requirements for cracking by aiding specific adsorption.

The initiation of fatigue cracks at smooth surfaces may occupy as much as 90% of the total so-called fatigue-life in the absence of environmental interaction. Corrosive reactions have been known to reduce this proportion of the service life to less than 10%. The implication, therefore, is that contact with an appropriate environment has about the same effect in facilitating the progression to Stage II growth as does the introduction of a sharp geometrical discontinuity onto an otherwise smooth surface. There is no shortage of possible mechanisms whereby corrosion related processes could influence fatigue crack initiation [7]. There is however a marked shortage of definitive experiments and quantitative data that would allow the feasibility of these mechanisms to be assessed.

Two mechanisms of crack propagation by dissolution have been suggested for environmental cracking due to static loads depending

upon the presence or otherwise of structural features (e.g. segregate or precipitate) usually at grain boundaries which cause a local galvanic cell to be set up. In this context the precipitate or segregate may act as the anode in a local cell or as an efficient cathode causing attack to be localized in the immediately adjacent matrix material. The function of the applied stress in such a system is presumably to prevent the dissolution reaction from becoming stifled by film formation. When pre-existing active paths are non-existent, or are inoperative because of environmental effects, the stress may act to disrupt a protective film formed on the metal surface to expose bare metal and so maintain relatively high localized anodic current densities at the exposed surface.

Crack propagation by dissolution mechanisms involves liquid diffusion of either solvating water molecules or aggressive anions down the crack length to the sight of rupture of the protective oxide, at planes of slip step emergence at the crack tip, followed by dissolution of the newly created metal surface. Ford [8] carried out work showing that if the strain rate at the crack tip is insufficient to maintain a bare surface condition, then crack propagation rates will be below those predicted by the dissolution mechanism. Conversely, when the crack tip strain is too high, mechanical crack advancement may dominate due to ductile rupture at the crack tip. At some intermediate value of crack tip strain rate optimum conditions for environmental enhanced growth will exist [8].

Hydrogen embrittlement has also been proposed as a failure mechanism [38] and adsorbed hydrogen may embrittle materials in one of two ways:

1. Directly by adsorption at the crack tip and lowering the surface energy of the material, $\gamma$, and thereby lowering the fracture stress of the material.

2. Indirectly by diffusing to some region in advance of the crack tip where the stress or strain conditions are particularly favourable for the nucleation of cracks, e.g. at regions of maxi-

mum stress triaxiality usually considered to be located at the elastic plastic interface of the plastic zone formed at the crack tip.

However, more important than the detailed mechanism of hydrogen embrittlement is whether environmentally assisted crack growth in aqueous environments is principally assisted by metal dissolution or by hydrogen embrittlement. In order to understand which of these environmental factors is mainly responsible for the enhanced crack growth in corrosion fatigue, it is necessary to recognize that the electrochemical conditions within the confines of a propagating crack may be significantly different from those at the surfaces exposed to the bulk environment.

It is conceivable that the electrode potential distribution within a crack enclave may vary with its depth and that the composition of the solution within the crack may be very different from that of the bulk solution. This may, for example, explain why the initiation stage of cracking is not necessarily circumvented, when precracks are introduced into stress corrosion or corrosion fatigue specimens. Initiation may involve the establishment of certain electrochemical conditions within the crack enclave which are appreciably different from those of the external surfaces. Not only can compositional variations be set up in a crack, but potential drops down cracks can also be developed [9]. It seems that whether or not significant potential drops are likely to exist along the length of growing cracks, will depend upon whether or not high net currents can be maintained between specimen and counter electrode. Any tendency for the material to form a continuous passivating film precludes the development of large potential drops since the active crack tip will be passivated. It should therefore be possible to predict which control potentials are conducive to the development of large potential drops down the length of cracks or crevices, by inspection of the appropriate polarization diagrams for the metal-environment combination [9].

Gabetta and Rizzi [10] measured electrochemical potentials at the tip of a growing fatigue crack in demineralized water at 93 °C.

The effect of frequency, waveform and oxygen content were investigated on A 533 B Class 1 steel. During the tests two probes were inserted in the specimen in two parallel holes drilled in the crack plane ( Fig. 2.3).

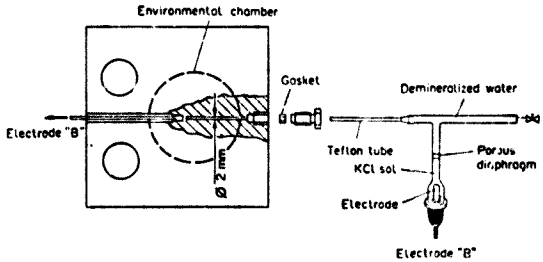


FIGURE 2.3: Electrode assembly after Gabetta and Rizzi [10].

The central hole ('A') was internally coated by an insulating lacquer. Probe 'B' was moved during the test to follow the crack front position. Another Teflon probe ('C') was positioned far away from the crack, in the machined notch.

Crack length and potential values measured by the three electrodes are shown in Fig. 2.4 where the various oxygen contents are shown.

Potentials recorded by probe A, during periods 2, 3 and 4 show that the probe was no longer able to follow the crack front potential. Probe B shows that the potential increases with an increase in dissolved oxygen. The value of the potential measured close to the specimen notch was assumed as a reference value. In period 1 probe C measured active potentials indicating that the oxide formed was not protective. As oxygen contents increased larger differences were observed in potentials for probes "b" and "c". This shows that the external surface had passivated. The different frequency and waveform experiments [10] showed that for high oxygen levels (period 2), the difference in potential due to the loading (maximum

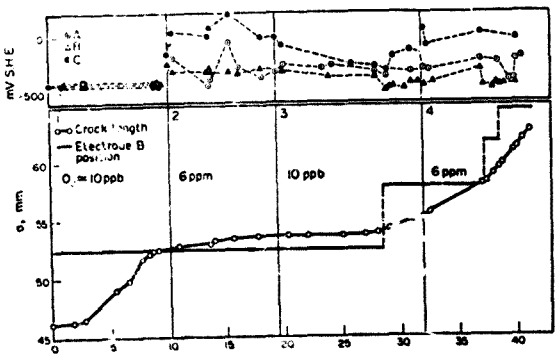


FIGURE 2.4: Crack length and potentials as functions of elapsed cycles. The four periods are also included

versus minimum load) was larger (up to 60 mV) than for low oxygen levels. This was attributed to a 'pumping' effect and to oxygen consumption by chemical reaction inside the crack. A plot of load and potential versus time is shown in Fig. 2.5. In this case the oxygen content is about 200 ppb at maximum load, and up to about 300 ppb when the crack closes. This appears to imply that when the crack is open, the oxidation reactions (which decrease the oxygen content), overrule the pumping effect (which increases the oxygen content).

When corrosion takes place on metal surfaces exposed to a small volume of solution and where access of fresh electrolyte and dissolved gases is restricted, the composition of the solution within the crack may change markedly from that of the bulk solution. Evans [12] has suggested that local acidity can develop due to hydrolysis of metal ions in solution according to reactions such as:

$$3Fe^{2+} + 4H_2O \rightarrow Fe_3O_4 + 8H^+ + 2e.$$

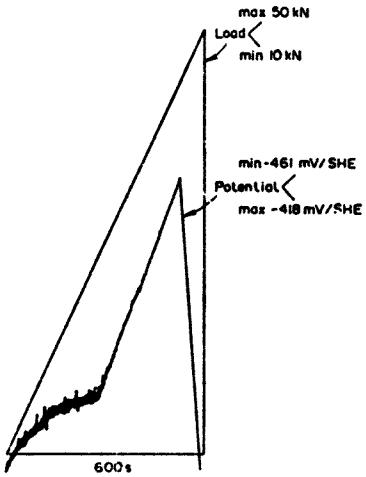


FIGURE 2.5: An example of potential variation with loading during period 4 [10].

It can be predicted that hydrolysis will cause the crack tip pH or pH within a pit to equilibrate at around 3.5 when iron is exposed to an aqueous environment at the free corrosion potential. The actual pH development depends upon the exact nature of the hydrolysis reactions taking place within the crevice.

The significance of both a change in the pH and potential of the metal at the crack tip on possible crack propagation mechanisms can be deduced if the relevant experimental data, plotted on the appropriate pH diagram for the system under investigation .Figure 2.6, for example, shows the influence of cathodic polarization on the potentials and pH values developed within a simulated pit in a carbon steel immersed in 0.001 M NaCl of pH 10 (Pourbaix). The extent and directions in which the potential and pH in the simulated pit change are dependent upon the degree of polarization applied to the

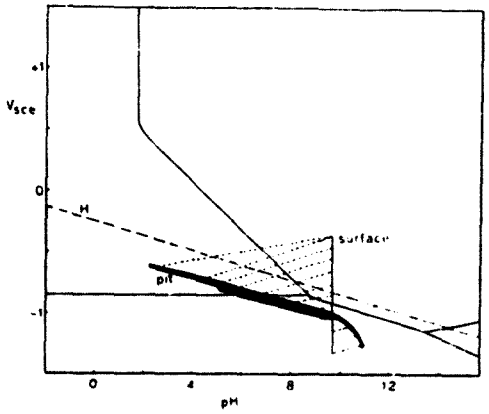


FIGURE 2.6: Influence of cathodic polarization on the electrochemical characteristics of a corrosion pit or crevice (carbon steel in the presence of an aerated solution of NaOH 0.001 M and NaCl 0.001 M). From Pourbaix.

steel surface external to the pit. The potential within the pit however always falls below the line representing the discharge of hydrogen from water.

Although the above remarks refer to measurements made in pitting or stress corrosion situations they should also be applicable to corrosion fatigue cracks. The main difference with corrosion fatigue is that the solution is pumped into and out of the crack producing regular mixing of the crevice solution with the bulk solution [12], thus reducing local polarization effects.

### 2.1.3 The Prevention of Corrosion Fatigue [13]

There are two possible approaches to attempting to prevent the occurrence of corrosion fatigue failure in structures. Firstly, the

engineering approach in which the working stresses to which the material is to be subjected are limited so that the stresses never (or rarely) exceed those corresponding to some corrosion fatigue threshold during the lifetime of the component. Secondly, in the electrochemical approach, attempts are made to change the environmental conditions by controlling the applied potential, using inhibitors, or applying coating systems so that the damaging corrosion reactions are less likely to occur.

A method that can be used to prevent corrosion fatigue crack initiation is cathodic protection. Cathodic protection is a remedial measure that can raise the fatigue limit of a material exposed to a corrosive environment to the corresponding fatigue limit in vacuo. Cathodic protection can be achieved either by coupling the structure to be protected to a metal more base in the electrochemical series, or by applying a cathodic current to the structure via an external source such as a battery or D.C. generator. Care is required so that overprotection does not lead to hydrogen charging which could result in hydrogen embrittlement. An alternative form of protection which has found considerable application in preventing stress corrosion cracking is anodic protection. This technique relies on the development of a protective passive film on the surface of the material by the application of an anodic current from an external source, usually a potentiostat. In the absence of chlorides, improvement is greatest with materials such as stainless steels and titanium alloys which rely on a highly protective oxide for their corrosion resistance. It is also possible to consider changing the composition or structure of an alloy to improve stress corrosion or corrosion fatigue resistance. This has been the subject of some research but it has usually been found that metallurgical solutions are not economically viable.

Since inhibitive treatments are usually costly, they are normally applied only in closed systems in which the corrosive environment forms the working fluid, e.g. in boilers or heat exchangers. The nature of the inhibitor employed varies according to the metal and corrosive environment concerned but, in general, all inhibitors are effective either by reacting with the products of the corrosion

reactions occurring on the metal surface or by adsorbing onto the metal surface and thereby forming insoluble protective films. If a sufficiently high concentration of inhibitor is not maintained then intensified highly localized action may result [14].

## 2.2 AN ASSESSMENT OF THE INTEGRITY OF P.W.R. PRESSURE VESSELS

The integrity of the thick walled steel reactor pressure vessel (R.P.V.) of a pressurized water reactor (Fig. 2.7) is vital for safety for two reasons. Firstly the R.P.V. is the container for the reactor core. Should the R.P.V. develop a leak and if the rate of loss of coolant exceeds the maximum capability of the emergency cooling water system, then the reactor core could become uncovered, overheated, and unless some remedial action was immediately undertaken, ultimately melt. Secondly, a massive failure of the R.P.V. itself could both seriously damage the reactor core and, at the same time, could damage the containment building.

In this way a single postulated event could possibly outflank the various sequential barriers which prevent the escape of fission products in other postulated accident sequences, namely, the fuel cladding, the primary circuit and possibly the containment building. Therefore it is important to demonstrate that the disruptive failure of a R.P.V. has a low probability bordering on the inconceivable. Since such accidents could give rise to large controlled releases of radioactivity, the R.P.V. disruptive failure probability must be, at least, less than one in a million reactor years, and preferably lower. A cumulative total of 10 000 reactor pressure vessel service years is not expected until about the turn of the century and, even that, will still be insufficient to gain confidence in failure probabilities, should there be any!

It has become apparent, during the UKAEA study [15] under the chairmanship of Dr W. Marshall, that there were no general principles which could be invoked to guarantee safety. Reactor pressure vessel integrity could only be established by careful attention to factors such as design, materials, fabrication, quality assurance,

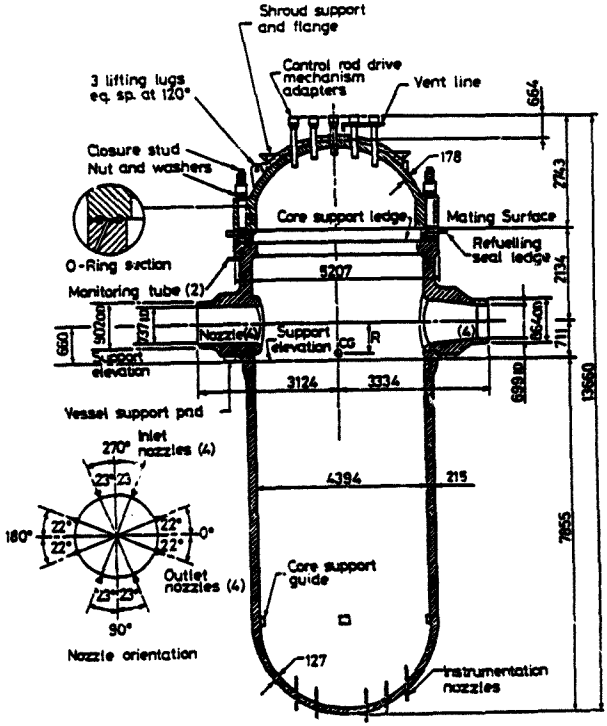


FIGURE 2.7: The reactor vessel of a 4-loop P.W.R. system (Dimensions given in millimetres) [15].

testing, inspection and so forth. Therefore the assessment of P.W.R. vessel integrity requires the combination of scientific and engineering analysis, metallurgical and engineering judgement, together with practical experience.

## 2.2.1 The P.W.R. Pressure Vessel

The primary function of the vessel is to contain the reactor core and primary coolant. It must do so under Level A, B, C and D Service Limits which are respectively, normal (e.g. plant heat-up and cool down), upset (e.g. reactor trip and loss of load), emergency (e.g. small loss of coolant, small steam line break or complete loss of flow) and fault (e.g. large loss-of-coolant or large steam line break) conditions [37]. Typical design parameters and mean operating conditions are:

| | |
|---|---|
| normal operating pressure | 15,98 MPa |
| design pressure | 17,13 MPa |
| initial hydraulic pressure | 21,42 MPa |
| normal operating inlet temperature | 288 °C |
| normal operating outlet temperature | 327 °C |
| design temperature | 343 °C |
| no-load temperature | 292 °C |
| design life | 40 yr at 80% load factor (32 effective full power years) |

The desirability of using steel plates and forgings of high toughness, adequate strength and weldability in thick sections, combined with good service experience, currently narrows the choice to a number of low alloy steels containing manganese, nickel and molybdenum. The composition, certain aspects of fabrication and the mechanical properties required of pressure vessel plates, forgings and welds are specified in the ASME Boiler and Pressure Vessel Code, Sections II, III and IX. The current choice of material is of specific SA-533 B alloys for plates and SA-508 alloys for forgings (Class 3 for improved weldability). SA-533 Grade B Class 1 is specified since it has the lowest range of tensile and yield strengths specified for SA-533 in order to achieve a relatively high upper shelf fracture energy and low ductile-brittle transition temperature.

It should be noted that the composition of SA-508 Class 3 material is very close to that of SA-533 B and in general therefore, conclusions drawn from experimental work on SA-533 B Class 1 steel are also pertinent to SA-508 Class 3 material and vice-versa [Table 2.1 and 2.2].

TABLE 2.1: Minimum Mechanical Properties Specified in the ASME Codes

| | A5338 1 Plate | | A508 3 Forgings | |
|---|---|---|---|---|
| | 20 °C | 350 °C | 20 °C | 350 °C |
| Tensile | | | | |
| Yield stress (MPa) | 345 | 285(*) | 345 | 285 |
| Ultimate tensile stress (MPa) | 522 | 527 | 550 | - |
| El (in 50 mm) % | 18 | - | 18 | - |
| R of A % | - | - | 38 | - |
| Charpy Impact | | | | |
| Energy (J) | 68 J at $RT_{NDT}$ + 33 °C | | | |
| Lateral expansion (mm) | 0.89 mm at $RT_{NDT}$ + 33 °C | | | |
| Minimum ave. value (+) of three specimens | x | | 41 J at 4.4 °C | |
| Minimum value of one specimen | x | | 34 J at 4.4 °C | |

(*) non-mandatory

(+) not more than one specimen from a set may fall below this value

x to be specified by purchaser

Since the plates and forgings have to be welded together in the fabrication of a vessel, it is obvious that the mechanical property requirements of the welds and the associated heat affected zones (HAZs) can be no less demanding than those of the plates and forgings, particularly as experience has shown these to be the most likely location for flaws.

The ASME requirements for weld mechanical properties and procedures are diverse, but are found mainly in Sections II, III and IX of the Code. They appear to be less specific than those for plates and forgings, but there is a requirement that all welds should conform

TABLE 2.2: Typical Compositions of Modern P.W.R. Pressure Vessel Steels [15]

| Material Specification | Country of Origin | No. of Analysis | Average Heat Analysis (Weight per cent) C | Mn | Ni | Mo | Si | Cr | P | S | Cu | Al | As | Sn | Sb | Co |
|---|---|---|---|---|---|---|---|---|---|---|---|---|---|---|---|---|
| SA533B Cl1 | Japan | 175 | 0.201 | 1.371 | 0.616 | 0.520 | 0.243 | 0.136 | 0.007 | 0.006 | 0.049 | 0.025 | 0.007 | 0.808 | 0.002 | - |
| SA533B Cl1 | USA | 13 | 0.216 | 1.367 | 0.547 | 0.547 | 0.236 | 0.074 | 0.009 | 0.014 | 0.117 | - | - | - | - | - |
| SA508 Cl3 20MnMoNi55 forging grade | Japan | 166 | 0.208 | 1.398 | 0.753 | 0.505 | 0.243 | 0.097 | 0.007 | 0.007 | 0.054 | 0.028 | - | - | - | - |
| | | 153 | - | - | - | - | - | - | - | - | - | - | 0.007 | 0.008 | - | - |
| | | 130 | - | - | - | - | - | - | - | - | - | - | - | - | 0.002 | - |
| | | 86 | - | - | - | - | - | - | - | - | - | - | - | - | - | 0.009 |
| SA508 Cl3 (etc.) | France | 125 | 0.16 | 1.338 | 0.722 | 0.503 | 0.236 | 0.195 | 0.010 | 0.010 | 0.065 | - | 0.016 | 0.011 | - | 0.017 |
| SA808 Cl2 | Japan | 64 | 0.208 | 0.803 | 0.844 | 0.585 | 0.231 | 0.374 | 0.006 | 0.006 | 0.048 | 0.029 | - | - | - | - |
| | | 58 | - | - | - | - | - | - | - | - | - | - | 0.009 | 0.008 | - | - |
| | | 34 | - | - | - | - | - | - | - | - | - | - | - | - | 0.02 | - |
| | | 20 | - | - | - | - | - | - | - | - | - | - | - | - | - | 0.010 |
| SA508 Cl2 | USA | 5 | 0.218 | 0.682 | 0.600 | 0.596 | 0.284 | 0.374 | 0.006 | 0.011 | 0.010 | - | - | - | - | - |

TABLE 2.2: Typical Compositions of Modern P.W.R. Pressure Vessel Steels [15]

| terial ecification | Country of Origin | No. of Analysis | Average Heat Analysis (Weight per cent) C | Mn | Ni | Mo | Si | Cr | P | S | Cu | Al | As | Sn | Sb | Co |
|---|---|---|---|---|---|---|---|---|---|---|---|---|---|---|---|---|
| 5338 C.1 | Japan | 175 | 0.201 | 1.371 | 0.616 | 0.520 | 0.243 | 0.136 | 0.007 | 0.006 | 0.049 | 0.025 | 0.007 | 0.008 | 0.002 | - |
| 5338 C.1 | USA | 13 | 0.218 | 1.367 | 0.547 | 0.547 | 0.236 | 0.074 | 0.009 | 0.014 | 0.117 | - | - | - | - | - |
| 508 C.3 | Japan | 166 | 0.200 | 1.398 | 0.753 | 0.505 | 0.243 | 0.097 | 0.007 | 0.007 | 0.054 | 0.028 | - | - | - | - |
| MnMoNi55 rging grade | | 153 | - | - | - | - | - | - | - | - | - | - | 0.007 | 0.008 | - | - |
| | | 130 | - | - | - | - | - | - | - | - | - | - | - | - | 0.002 | - |
| | | 86 | - | - | - | - | - | - | - | - | - | - | - | - | - | 0.009 |
| 508 C.3 Rc.) | France | 125 | 0.16 | 1.338 | 0.722 | 0.503 | 0.235 | 0.195 | 0.010 | 0.010 | 0.065 | - | 0.016 | 0.011 | - | 0.017 |
| 508 C.2 | Japan | 64 | 0.206 | 0.803 | 0.844 | 0.585 | 0.231 | 0.374 | 0.006 | 0.006 | 0.048 | 0.029 | - | - | - | - |
| | | 58 | - | - | - | - | - | - | - | - | - | - | 0.009 | 0.008 | - | - |
| | | 34 | - | - | - | - | - | - | - | - | - | - | - | - | 0.02 | - |
| | | 20 | - | - | - | - | - | - | - | - | - | - | - | - | - | 0.010 |
| 508 C.2 | USA | 5 | 0.218 | 0.682 | 0.600 | 0.596 | 0.284 | 0.374 | 0.006 | 0.011 | 0.010 | - | - | - | - | - |

to a of the minimum mechanical property specifications for the materials joined by weldments. This is clearly a desirable requirement.

The inner surface of the vessel is clad with a corrosion resistant layer by weld overlay cladding. The method is mechanized for single curvature surfaces in order to melt a layer of constant thickness, but certain regions of double curvature must be clad manually. Two types of feed material are used; an austenitic stainless steel which is used for cladding the ferritic steel of the main pressure vessel and Inconel 600 for penetrations, core support pads and on the faces of the nozzles. The Westinghouse Equipment Specification refers to the acceptability of the cladding in the post-weld heat treated condition. This implies that the heat treatment of the vessel shall in no way be modified to optimize the metallurgical state and corrosion resistance or mechanical properties of the cladding.

A potential problem associated with cladding of reactor pressure vessels is underclad cracking. First reported in 1970, it was found that discontinuities were formed in the HAZ of the ferritic steel base material, formed by the cladding process. A comprehensive study was undertaken and the results published by Vinckier and Pense in 1974 [16]. Cracks up to 3 mm deep were found, and in more recent reviews the maximum depth is 4 mm. The authors concluded that different steels have different susceptibilities to underclad cracking. No cracking was reported for SA-533B Class 1 material, one case was reported for SA-508 Class 3, and the remaining reported cases were for SA-508 Class 2 steel. This pattern has been confirmed by recent reviews. The cracking was all attributed to reheat cracking occasionally augmented by liquation cracking.

### 2.2.2 Fracture Assessment

The ultimate mechanical failure of a loaded metallic structure can occur in several ways. At one extreme, deformation can occur throughout the structural section resulting in a large dimensional

change and possibly shape changes. Alternatively, the deformation may begin homogeneously but become localized as the section thickness is reduced thereby increasing the effective stress under a fixed load. At the other extreme, the failure process may involve only a very small volume fraction of the structure, with deformation being extremely limited, resulting in the propagation of a crack across the material section without gross dimensional changes. Such a failure is termed 'brittle fracture' (Fig. 2.8). Both these modes of failure are strongly influenced by the presence of pre-existing cracks or flaws in the structure. It is therefore necessary to consider the conditions under which a vessel might fail by the unstable extension, under the applied stresses, of an assumed pre-existing crack. These conditions are conveniently represented by the size of defect which will propagate and ultimately become unstable at the stresses, temperatures, etc. to which the vessel may be subjected. The techniques used to calculate these sizes of defects and to characterize the material's resistance to failure by unstable crack propagation are collectively referred to as fracture mechanics.

In the first study group report [17], initiation defect sizes were estimated using the methods of 'linear elastic fracture mechanics' (L.E.F.M.). This method is based on elastic theory describing the stress, strain and energy fields ahead of cracks subject to external loading. The fields are described by the stress intensity factor, $K_I$. $K_I$ is related to applied stress ($\sigma$) and defect size 'a' by the equation -

$$K_I = Y\sigma \sqrt{\pi a} \qquad (2.5)$$

where Y is a dimensionless geometry factor. The initiation flaw size is therefore given by $K_{Ic}^2/Y^2\sigma^2\pi$.

As the basis of LEFM is the elastic behaviour of solids, $K_I$ and therefore $K_{Ic}$ only have significance when the plasticity is limited with respect to the crack length and remaining ligament. This in turn places limitations on specimen size for the determination of $K_{Ic}$. The range of application of LEFM may be extended

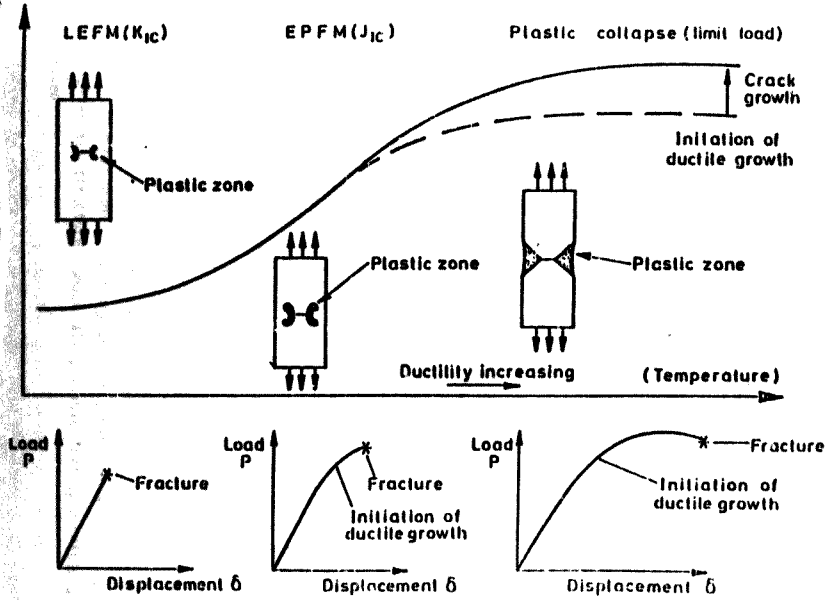


FIGURE 2.8: A simplified diagram of various fracture modes.

by the adoption of an 'effective crack length' derived by adding the estimated size of the plastic zone ahead of the crack tip onto the physical crack length. This procedure has been used to predict the initiation of crack propagation in structures of limited size, but LEFM becomes inapplicable at high net section stress levels (typically where the applied net section stress is greater than 80% of the yield stress) when the derived initiation crack sizes can be non-conservative because large-scale plasticity effects intervene.

The constructional steels used in the manufacture of pressure vessels have moderate yield strengths, combined with high ductility over a wide temperature range. The thickness and yield strength of P.W.R. vessel steels are such that if ultimate failure were to occur at normal operating temperatures, plasticity may not be limited and would probably occur over the entire remaining ligament. The problem of relating fracture to applied load and crack length under these conditions is described by means of 'elastic plastic fracture mechanics' (EPFM) (Fig. 2.8). Recently, standard test methods for the determination of EPFM parameters have been published but as yet, no internationally agreed procedures exist for their direct use in structural integrity assessment. One problem common to all EPFM approaches is in the treatment of stable crack growth occurring prior to final failure during ductile fracture at normal operating temperatures. When failure occurs under completely elastic conditions, the onset of crack propagation characterized by $K_{Ic}$ is usually coincident with instability and no possible ambiguity arises. However, under EPFM conditions the onset of crack growth can occur in a stable manner such that an increase in load or applied displacement is required to increase the spread of plasticity before the crack extends further. At present the data which exists to validate the assumption that the stable crack growth observed under laboratory testing conditions will also occur in full-scale structures under all possible loading conditions is limited.

### 2.2.3 Sub-critical Crack Growth

It is well known that the expected life of many engineering components or structures can be limited by the growth of initially sub-critical cracks to critical dimensions under the operating conditions. Such growth at temperatures below the characteristic creep range of the structural material can be broadly classified under two headings:

- Growth in inert environments due to the application of cyclic stresses, i.e. metal fatigue, and

- Growth in a chemically reactive environment due to the application of either cyclic or nominally static tensile stresses, i.e. corrosion fatigue and stress corrosion cracking respectively. A clear-cut distinction between the latter two failure mechanisms can no longer be made and environmentally induced or enhanced growth would be a better description.

The reactor pressure vessel is subject to fluctuating stresses as a result of both normal operation and the various tests and upsets likely to arise during its lifetime. Although transients include both pressure and temperature changes, there is no high frequency thermal cycling due to fluid mixing as encountered in other systems (e.g. B.W.R. feed nozzles). It is important to know whether sub-critical cracks which may be present initially could grow to a critical size by any slow crack growth processes.

#### 2.2.3.1 Fatigue crack growth in 'inert' environments

The only conceivable slow crack growth mechanism for 'dry' cracks in reactor pressure vessel steels (both bainitic steels such as SA533-B and SA508 and austenitic cladding steels), at operating temperatures usually below 320°C, is fatigue crack growth. To calculate the growth of postulated cracks in the reactor vessel, an equation is required to describe the rate of growth as a function of the number of occurrences and magnitude of the applied cyclic

stresses. From a fundamental point of view, the rate of crack growth should depend on the processes of plastic deformation at the crack tip and various models have been proposed on this basis [18-20]. Many of these models are associated with striation growth, so-called from the appearance of the fracture surfaces. Under conditions of small-scale yielding, the elastic stress field controls the plastic strain at the tip of a crack and the results of these theoretical models can be translated into functions of the linear elastic fracture mechanics parameter, $K_I$, and in particular, the cyclic stress intensity range, $\Delta K_I = K_{I,max} - K_{I,min}$, derived from the applied cyclic stress range.

For a wide range of $\Delta K_I$, the fatigue crack growth rate is given by:

$$\frac{da}{dN} = C(\Delta K_I)^n \qquad (2.6)$$

where C and n are constants. The theoretical predicted value of n usually lies in the range 2 to 4. This equation was first suggested as an empirical correlation [6] and its general form now has firm theoretical support. It is customary to represent experimental data in this way and it provides the means of calculating the progress of fatigue cracks in components through the linking mechanical parameter, $\Delta K_I$.

There are, however, limits to the range of $\Delta K_I$ when equation (2.6) is applicable. There exists for all materials a lower threshold of $\Delta K_I$ at which fatigue cracks can no longer propagate. There is also an upper limit where the maximum value of $K_I$ approaches the fracture toughness or tearing instability condition. For tough ductile materials, some ductile tearing occurs as instability is approached and a gradual acceleration of crack growth to fracture from that predicted by equation (2.6) is observed. The complete fatigue crack growth curve therefore takes the form shown in Fig. 2.9. Both the upper and lower limiting values of $\Delta K_I$ are lowered by increasing the mean tensile stress intensity about which the fatigue cycle oscillates, whereas the linear portion of Fig. 2.9 represented by equation (2.6) remains relatively unaffected

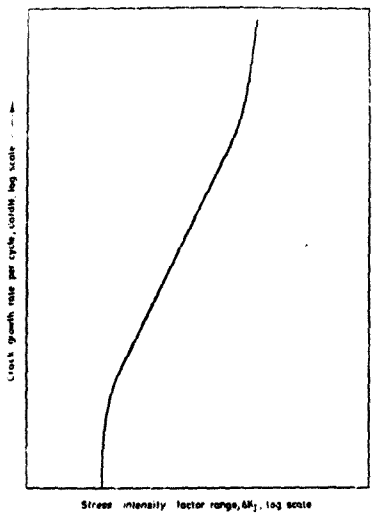


FIGURE 2.9: Schematic representation of fatigue crack growth rates, da/dN (crack extension per cycle), as a function of $\Delta K_I$ [15].

(for the case of inert environments). The mean stress or stress intensity level in the fatigue cycle is usually represented in terms of the stress ratio, $R = \frac{K_{min}}{K_{max}}$.

In relatively inert environments such as dry air, the form and quantitative relationship of Fig. 2.9 is surprisingly invariant to metallurgical variables and mechanical variables such as frequency and stress wave shape. However, the same cannot be said for more chemically reactive environments. Establishing a safe, but realistic crack growth equation of the form of Equation (2.6) in order to carry out calculations on a reactor pressure vessel can be a difficult task and in some instances for wet cracks, described later, contributes the greatest uncertainty to the calculations.

2.2.3.2 Fatigue crack growth in P.W.R. environments

In the first study group report [17], the validity of the ASME Section XI Appendix A Code recommendation for the upper bound crack propagation curve for dry sub-surface cracks was questioned, particularly for high R ratio cycles, and the 'High R Dry' crack growth curve substituted. These curves are shown in Fig. 2.10. (For the purpose of this part of the discussion, air, even at 300 °C, is assumed inert as far as crack propagation is concerned. This is not strictly correct but the errors arising are considered small.) The 'High R Dry' curve takes into account known crack propagation data at comparatively low values of the cyclic stress intensity factor, $\Delta K$. In fact, fatigue crack propagation in air in SA533-B and SA508 steels and typical weldments is comparatively well categorized. The range of variables covers frequencies from 0.17 to 160 Hz, temperatures from 20 to 300 °C, specimen thickness from 5 to 100 mm, stress ratio from 0 to 0.8 and neutron irradiation up to total doses of $5.7 \times 10^{19}$ neutrons/cm$^2$ ($E > 1$ MeV) [21-23]. None of these variables has significantly increased or decreased crack growth rates outside the scatter band observed in room temperature air and whose upper bound is represented by the "high R Dry' curve. This result is expected because fatigue crack growth in ductile steels is not strongly influenced by composition or microstructure provided that the normal ductile striation mechanism operates and, that no alternative severely embrittled pathways exist.

The more recent results of the U.K.A.E.A. experimental programme on SA533-B steel in an inert helium environment at 288 °C, shown in Fig. 2.11, also suggest that the ASME Section XI Appendix A Code growth curve for dry cracks does not represent an upper bound [15]. For predictions of dry crack growth, an adequate representation of these results is:

$$\frac{da}{dN} = 1 \times 10^{-11} \Delta K^3 \text{ metres/cycle } (\Delta K \text{ in MPa } m^{1/2}) \qquad (2.7)$$

which is identical with a proposed upper bound to data for several pressure vessel steels reviewed several years ago [24].

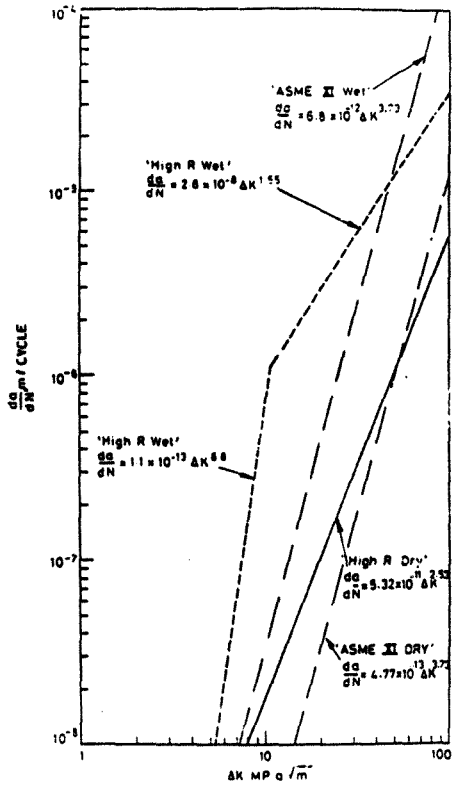


FIGURE 2.10: The ASME XI (1974) and high R (1976) fatigue crack growth equations [15].

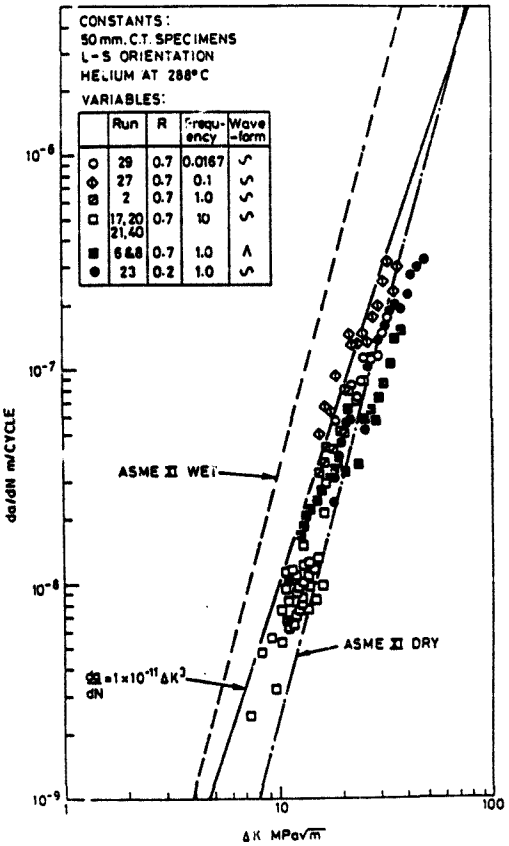


FIGURE 2.11: UKAEA crack propagation data for A533-B steel in helium at 288 °C [15].

From the general form of Fig. 2.9, an R ratio dependent lower crack growth threshold would be anticipated and has been observed [21, 24]. However, at high R ratios of 0.5 to 0.8 and low values of $\Delta K$, there is evidence to define a limiting fatigue crack growth threshold. This limiting value of $\Delta K_t = 2$ MPa.m$^{1/2}$ (in common with other ferritic steels) has been observed at room temperature at 288 °C, independent of R for values in excess of about 0.8 [21]. Therefore equation (2.7) is only applicable for values of $\Delta K$ in excess of 2 MPa.m$^{1/2}$. As might be anticipated, when this value is substituted in equation (2.7), the resulting value of da/dN is about one atomic spacing.

## 2.3 ENVIRONMENTAL CRACKING

Ferritic iron-base alloys react in pure deaerated, high temperature water to form a protective oxide film based on magnetite, $Fe_3O_4$. In P.W.R. primary water at 300 °C, the austenitic cladding corrodes at only a slightly lower rate than the base material. This is in contrast to the considerable differences in corrosion behaviour of the two materials in aerated water at room temperatures. P.W.R. primary water is treated with three additives: Molecular hydrogen to getter radiolytic decompostion products of water, lithium hydroxide to increase the solution pH and thus lower the general corrosion rate, and boric acid for nuclear reactivity control (boron has a large surface area for neutron adsorption). It is common knowledge that dissociation of water in boric acid solutions under reactor irradiation could be suppressed by $H_2$ in the coolant. The required hydrogen concentration increases with boron fissioning rate (boric acid concentration). The boron constituent varies over a very wide concentration range of 10 g/ml with new nuclear fuel to zero at the end of a fuel cycle. This does not seriously affect the corrosion rates of austenitic or ferritic steels at high temperatures because the acid associates with increasing temperature. This again is in contrast to room temperatures, where ferritic pressure vessel steels would corrode rapidly in the boric acid solution [25].

The quality, tenacity and rehealing (passivation) properties of the oxide film are of great importance in environmental cracking and

can be influenced by details of the water chemistry and microstructural features of the steel. In the latter category, localized segregation of a second phase, such as manganese sulphide inclusions, or of any element in a continuous network having significantly different electrochemical properties from the matrix, can produce a highly active dissolution path over which the protective oxide film may not properly form. Similarly, applied strains above a certain threshold, whether static or dynamic, can also break the oxide film, which under adverse electrochemical conditions will not reheal, resulting in environmental cracking. These two categories just described are called pre-existing active path dissolution and strain-generated active path dissolution.

In addition to these dissolution processes at sites of fractured oxide films the electrochemical theory of corrosion dictates that an equal amount of charge must be passed in a corresponding cathodic reaction. In the absence of oxygen, this will be a hydrogen evolution reaction. The effective hydrogen pressure at the corroding surface is several orders of magnitude greater than that of hydrogen deliberately added to P.W.R. primary water. Thus, in principle, if hydrogen enters the steel, embrittlement is a possibility. However, with steels of the type and strength level used in the pressure vessel, hydrogen induced crack growth is unlikely, particularly at temperatures in excess of 100 °C.

### 2.3.1 Corrosion Fatigue Data

Very little corrosion fatigue data for pressure vessel steels in P.W.R. water was available prior to the First Study Group Report [17], but what there was, clearly indicated a marked enhancement of the rate of crack propagation if the cyclic frequency was low (e.g. 0.0167 Hz) and the stress ratio was high (e.g. R = 0.7). The high R ratio data, in particular, exceeded the 'ASME Wet' crack growth curve and the 1978 Addendum to ASME XI restricted the use of the ASME XI Wet curve (Fig. 2.10) to cycles with stress ratios $R < 0.2$. These few results led to the 'High R Wet' upper bound curve shown in Fig. 2.10 and this equation was used for the first study group

report [17] to evaluate the growth of wet cracks in the P.W.R. pressure vessel independent of the nominal R ratio of the reactor transient considered. This was partly because the nominal R ratio was difficult to estimate and partly because the level of residual tensile stress present after stress relief, which could increase the effective R ratio, was also not known precisely.

The most recent review of the results from Westinghouse shows that this position has not changed significantly (Fig. 2.12). Crack growth also for simulated P.W.R. primary water conditions are shown in this figure derived from more than thirty specimens manufactured with a variety of orientations from SA-533B plate, SA-508 Class 2 steel and weldments thereof. At high R ratios in particular, the data for each specimen often falls on a characteristic 'hook-shaped' curve on a log da/dN versus log $\Delta K$ plot, the upper part of which is referred to as a 'plateau', indicating da/dN almost independent of $\Delta K$.

Fatigue striated fracture surfaces have been consistently reported in these experiments and this observation has been independently verified in fractographic examinations of Westinghouse specimens by the UKAEA. This indicates that during crack advance, the material is behaving in an apparently ductile manner which would be consistent with a combined fatigue/dissolution mechanism. In a series of experiments at room temperature in boric acid solutions, brittle cleavage facets have been observed in SA-533B steel [26]. Nevertheless, the crack growth rates were only marginally greater than those predicted by the old 'ASME XI Wet' curve (1974).

Present shortcomings appear to be that neither the frequency nor the R ratio effects on crack growth rates have been systematically examined to determine their most adverse combination. There is therefore no guarantee that a near upper bound curve to the present data represents a worst case for the simulated P.W.R. conditions tested. It should be noted that these data do not cover the full range of reactor transients with respect to loading rate and R ratio.

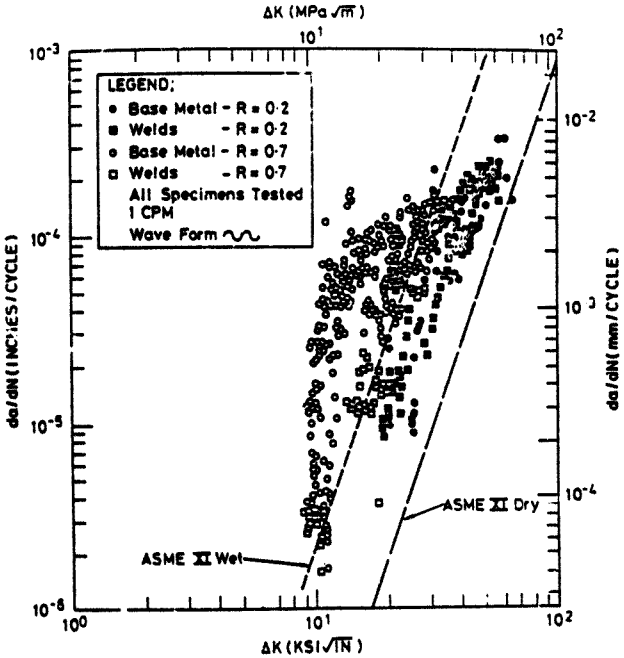


FIGURE 2.12: Corrosion fatigue data from Westinghouse for A533-B-1 and A508-2 base metals and weldments in P.W.R. primary water [15].

To date, some of the testing variables that have been investigated include different parameters on metallurgical, mechanical and chemical factors. The metallurgical parameters are the range of the chemical compositions of the materials (essentially the sulphur and carbon contents), and the nature of the products as determined by the processing conditions (rolled and forged steels). The mech-

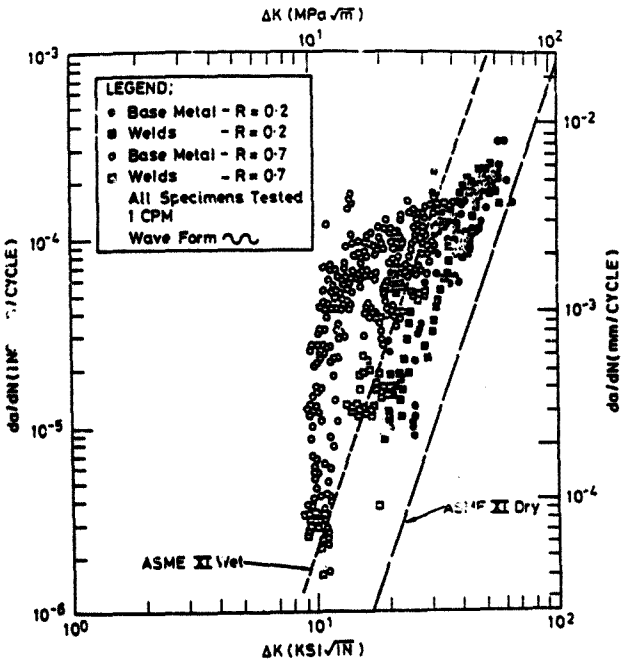


FIGURE 2.12: Corrosion fatigue data from Westinghouse for A533-B-1 and A508-2 base metals and weldments in P.W.R. primary water [15].

To date, some of the testing variables that have been investigated include different parameters on metallurgical, mechanical and chemical factors. The metallurgical parameters are the range of the chemical compositions of the materials (essentially the sulphur and carbon contents), and the nature of the products as determined by the processing conditions (rolled and forged steels). The mech-

anical parameters are the load ratio R, the waveform, the frequency and the loading (increasing or decreas[illegible] ΔK).

Amzallag et al. [27, 28] tested both SA508 Cl3 (forged steel) and SA533-B-1 (rolled steel) pressure vessel steel in two environments (C1 and C2). The C1 environment was pure water without additives, whereas C2 contained boric acid and lithium hydroxide additions. In both cases the oxygen, chloride and fluoride levels were very low viz below 0.10 ppm $O^2$ and 0.15 ppm $Cl^-$, $F^-$. Testing was carried out at temperatures of up to 300 °C, 140 bar pressure and the tests were performed in static autocalves. Table 2.3 shows the test matrix and the parameters studied include: (1) The sulphur level: between 0.009 and 0.018%; (2) Th[illegible]eform: triangular and sinusoidal at [illegible] 2 and R = 0.6. [illegible] ency: between 0.1 cpm and 5 Hz: [illegible] loading: [illegible] decreasing ΔK.

TABLE 2.[illegible] Test Ma[illegible]ix

| PARAMETER | MATERIAL | FREQUENCY | WAVEFORM | R RATIO | SULFUR LEVEL % |
|---|---|---|---|---|---|
| Reference Tests | A508 Cl3 A533-B- | [illegible]60 cpm | Triangle | 0.2 | 0.005 - 0.009 0.013 |
| Sulfur Content | A50[illegible] A53[illegible] | [illegible] cpm | Triangle Sinus | 0.2 | 0.009 - 0.013 0.019 |
| Waveform | A508 Cl3 A533-B-1 | 1 cpm 5-10 Hz | Triangle Sinus | 0.2-0.6 | 0.009 - 0.013 |
| R Ratio | A508 Cl3 | 1 cpm 1-10 Hz | Triangle Sinus | 0.2-0.6 [illegible].9 | 0.006 - 0.009 0.0[illegible]13 |
| Frequency | A508 Cl3 A533-B-1 | 0.1-1 cpm 5 Hz | Triangle Sinus | [illegible] 0.7-[illegible] | 0.006 - 0.009 0.013 |
| Loading increasing or decreasing ΔK | A508 Cl3 | 1 cpm | Sinus | 0.2 | 0.014 |
| Material Variability | A508 Cl3 A508 Cl3 (VCO) A50[illegible] Cl3 A | 1 cpm | Sinus | 0.2 | 0.006 - 0.013 0.014 |

Reference tests were conducted with a triangular waveform (R = 0.2) at frequencies of 1 and 60 cpm on material having sulphur contents in the range 0.005 - 0.013% (Fig. 2.13). For the two steels it was found that a slight, but significant effect of the P.W.R. environment was observed (relative to air data). The results for the two steels are very similar.

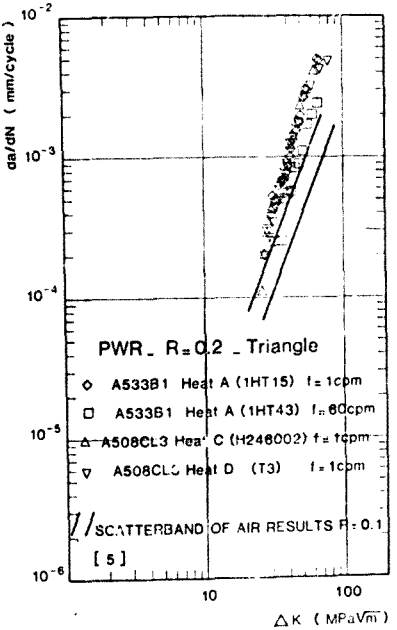


FIGURE 2.13: Effect of various heats of 508 and 533 material on the fatigue crack growth rate.

Amzallag's work revealed the following:

1. The fatigue crack growth rate (F.C.G.R.) of SA533-B steel (S = 0.018%) is higher than that of the steels having sulphur levels below 0.014%. The da/dN - $\Delta K$ curve exhibits a plateau-like shape (low slope).

2. The two waveforms give significantly different results for the material containing S = 0.013% with R = 0.2. The triangular waveform results in a typical fatigue type behaviour. The sinusoidal waveform leads to a stress corrosion-type behaviour with a rapid increase of the growth rate followed by a plateau (Fig. 2.14). For the low sulphur steels the effect of waveform was less pronounced. The effects of different waveforms (sinusoidal, triangular, sawtooth, trapezoidal) have already been examined by Cullen et al. [29] and by Bamford et al. [30]. These authors have also shown that the sinusoidal waveform is the most detrimental.

3. The effect of R ratio (0.2; 0.6; 0.9) was studied in low sulphur steels (S < 0.010%). It was shown that, for these test materials and test conditions, both the P.W.R. environment and the load ratio R have only a limited influence on the crack growth rates.

4. The effect of frequency was also examined by performing tests at frequencies ranging from 0.1 cpm to 5 Hz, on low S content material (S<0.010%). The results obtained did not show a significant effect of very low frequencies (f = 0.1 cpm).

5. The results obtained by increasing and decreasing $\Delta K$ were similar within the $\Delta K$ range investigated. It therefore seems that the high slope regions, relative to the onset of corrosion fatigue are independent of loading.

6. Metallurgical examinations revealed that when the crack growth rates are high and the curve presents a plateau-like shape

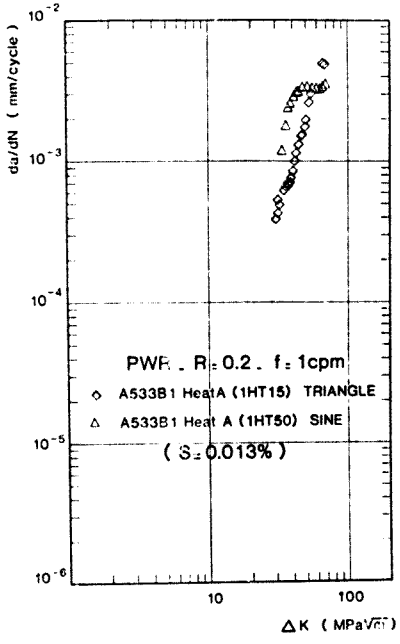


FIGURE 2.14: Effect of waveform on the crack growth rate of A533-B-1 material [27].

(high sulphur materials), the fracture surface is a 'brittle' type. Moderate increases in F.C.G.R. (medium sulphur steels) corresponded to local brittle features especially around MnS inclusions. When the crack growth rate in P.W.R. enviroments is only slightly higher than in air, the fracture surface consists mainly of ductile striations.

One of the most important parameters determining the F.C.G.R. was seen to be the sulphur content. Estimations of the increase of the F.C.G.R. as a function of the sulphur content are plotted in Fig. 2.15 by combining the results of several sources [30 - 33]. An increase in the ratio da/dN (P.W.R.) ÷ da/dN (ASME air) with the sulphur content and a relatively wide scatterband around the mean curve is observed.

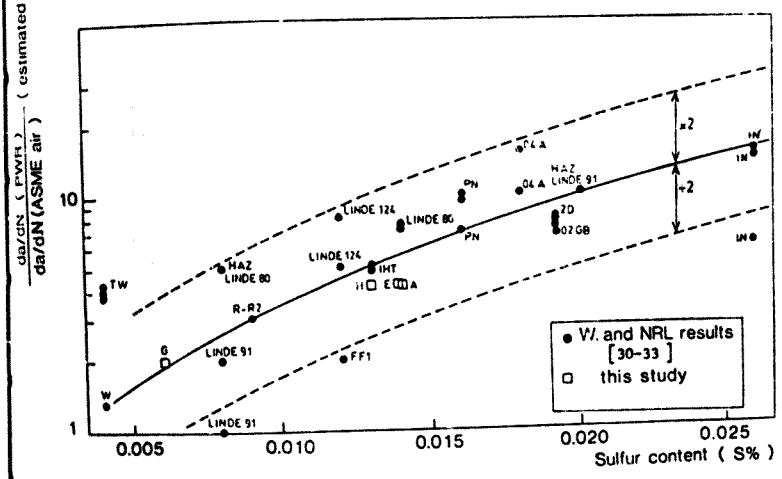


FIGURE 2.15: Accumulated results of variations in crack growth rates in P.W.R. environments (with respect to air environments) for given sulphur content steels [27].

Scott and Truswell [34] studied the effect of simulated P.W.R. environments on the corrosion behaviour of several ferritic pressure vessel steels. These included A533-B and A 508 C.3. In a previous paper [35], Scott described an extensive study of the influence of various water chemistry variables within the range permitted in

both P.W.R. and B.W.R. reactors on the rate of corrosion fatigue crack growth in A533-B steel. It was found that in P.W.R. water, pure water and B.W.R. water (at normal oxygen levels i.e. <10 ppb) there was very little environmental influence on the rate of crack growth when compared with an inert helium environment at 288 °C. These experiments covered a range of stress ratios between 0.2 and 0.7 and cyclic frequencies as low as 1 cpm (0.017 Hz). However, a large environmental effect was obtained in Scott's experiments at higher cyclic frequencies of the order 1 to 5 Hz, and R ratios of 0.7 to 0.9. It was argued [35] that the environmental influence was due to the operation of a dissolution-controlled stress corrosion process. Its suppression at lower cyclic frequencies was believed to be due to a fast passivation rate which competed with the rate of mechanical oxide rupture and prevented significant crack tip dissolution at all but the highest cyclic frequencies. The factors controlling the passivation rate could differ between experimental rigs and lead to a different response of crack growth rate to cyclic frequency. These could be related to either the water chemistry, or steel metallurgy and microstructure, or to both simultaneously. However, since no water chemistry variable within the normal range permitted in P.W.R. or B.W.R. systems was observed to cause substantial environmental effects in A533-B steel at low frequencies in Scott's experiments, attention has increasingly been focussed on metallurgical variables, especially steel sulphur content.

Scott and Truswell [34] were concerned with the effect of various metallurigcal variables, i.e., different heats of A533-B steel and other pressure vessel steels, on crack growth rates when immersed in P.W.R. primary water at 288 °C. The testing was carried out in autoclaves that gave turbulent conditions in the vicinity of the fatigue specimens (flowrates of 40 ℓ/min). Sample compositions, properties and orientation with respect to the rolled or forged product are shown in Table 2.4 and Fig. 2.16.

Steel samples were interchanged between Harwell and Westinghouse laboratories, and it was soon evident that the Westinghouse data

TABLE 2.4: Composition (percent) and mechanical properties at 20 °C of SA533 grade B class 1 steel [34]

| Heats | | A | B | C |
|---|---|---|---|---|
| Orientation | | L-S | L-S | L-T |
| Cast No. | | C8938 | 63758.1 | HSST-02 |
| Country of origin | ASME Specification | UK | France | USA |
| Carbon | 0.25(max) | 0.21 | 0.185 | 0.22 |
| Manganese | 1.10-1.66 | 1.24 | 1.395 | 1.45 |
| Phosphorus | 0.035(max) | 0.016 | 0.010 | 0.011 |
| Sulphur | 0.040(max) | 0.012 | 0.006 | 0.019 |
| Silicon | 0.13-0.32 | 0.20 | 0.195 | 0.22 |
| Molybdenum | 0.41-0.64 | 0.49 | 0.485 | 0.53 |
| Nickel | 0.37-0.73 | 0.66 | 0.655 | 0.69 |
| Chromium | - | 0.08 | 0.130 | 0.12 |
| Vanadium | - | - | - | - |
| Copper | - | 0.09 | 0.095 | - |
| Aluminium | - | - | 0.022 | - |
| Cobalt | - | 0.013 | - | - |
| Tin | - | 0.012 | - | - |
| Tantalum | - | <0.002 | - | - |
| Tensile strength, MPa | 552-689 | 571-601 | 607-612 | 594 |
| yield strength (0.2 percent offset), MPa | >344 | 398-408 | 468-472 | 405 |
| Elongation in 50 mm, percent | >18 | 23-25 | 28-29 | 16.5 |
| Reduction of area, percent | | 62 | - | 64 |

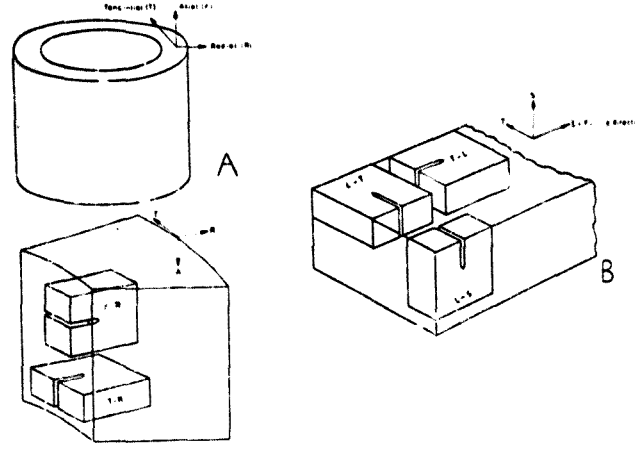


FIGURE 2.16: Specimen orientations from (A) forged cylinders and (B) rolled plates [34].

led to results greater than those of Harwell (by approximately 10 x, given $\Delta K$). It was therefore postulated that differences in results were probably not due to MnS stringer effects.

From a mechanistic point of view Scott discussed why several rigs showed different crack growth rate results. He concluded that crack growth rates are dependent on a competition between cyclic rupturing of the protective, passivating oxide film at the crack tip and its repair by passivation. It is believed that the electrochemical conditions which govern the rates of dissolution and passivation may be different in different experimental rigs and hence give rise to the observed variations in the influence of cyclic frequency, in particular. The electrochemical potential of the specimen is probably the crucial controlling parameter, and this will be set by factors such as water chemistry, water flowrate and steel metallurgy.

Atkinson and Lindley [36] studied the effect of frequency and temperature on the crack propagation of En56C (a martensitic stainless steel) and A533-B-1 a low alloy pressure vessel steel. Testing was carried out in vacuum, laboratory air, distilled water and neutral 3% NaCl.

Some of the conclusions drawn from this work were:

1. Crack growth rates in air (En56C) are 3 - 6 times greater than those in vacuum, although there is little effect of frequency on fatigue crack growth in air. A similar conclusion was drawn for A533-B-1 pressure vessel steel.

2. It is clear for both steels that the aqueous environmental enhancement of fatigue crack growth rates increases as the frequency of testing was decreased, using either sine or triangular waveforms over the $\Delta K$ ranges shown. It was found that maximum growth rates occurred at a 'peak' frequency: 0.025 Hz at 90 °C for A533-B-1 at a $\Delta K$ of 50 $MN.m^{-3/2}$.

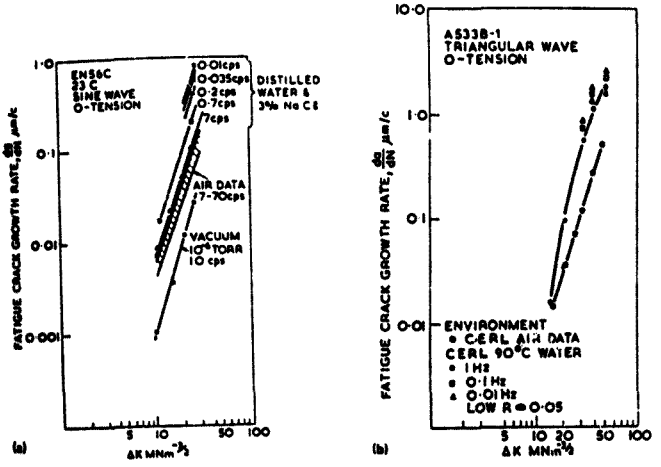


FIGURE 2.17(a): Effect of ΔK and frequency on growth rates in En56C
(b): Effect of ΔK and frequency on growth rates in A533-B-1 [36].

3. Distilled water and the 3% NaCl environment at open circuit potential led to enhancement of fatigue crack growth rates.

4. Square wave or negative sawtooth loading [36] at 0.1 Hz reduced the fatigue crack growth rate almost to the level observed in air. Triangular and positive sawtooth waveforms led to the same environmental enhancement of fatigue crack growth rate.

5. In all the experiments carried out it was found that the F.C.G.R. increased with increasing test temperature in the range 20 - 90 °C.

Mager et al. [37] have also studied the fatigue crack growth characteristics of A533-B-1 plate in P.W.R. and B.W.R. environments. The fatigue crack growth data for the five specimens tested either in air or in P.W.R. and B.W.R. primary grade reactor water at 288 °C and at 1 cpm are summarized in Fig. 2.18. From these results it can be seen that:

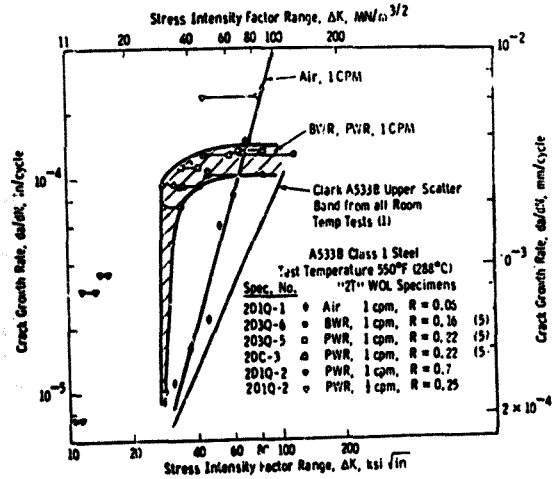


FIGURE 2.18: Crack growth rate, da/dN, versus ΔK for A533B steel showing the effect of environment, frequency and R - ratio [37].

The plateau region would suggest that all the implications of the existence of a static load stress corrosion condition, derived from the fatigue results, could be incorrect. Mager explains that the lower crack growth rates, at high ΔK, for P.W.R. and B.W.R. environments could be due to crack branching. In the absence of a plateau region, crack branching is

self limited due to decreasing K at the tip when a branch forms, and the high K dependence of the crack growth. Within the plateau region, the strong ΔK dependence no longer exists, and when the applied ΔK level is sufficiently high, then macro-branched cracks have sufficient driving force to allow propagation. Tests carried out in hydrogen sulphide showed no macro-cracks and therefore no plateau. The macrobranching has been found to depend strongly on the material being tested in that branching has not been observed in forgings, and seems to be limited to plate material.

Fractography revealed that the only crack growth mechanism was by ductile striation growth. This agreement held for all values of R ratio and cyclic frequency.

Hänninen et al. [38] presented an interpretation of the experimental data based on a hydrogen-induced cracking model. The material used was I.C.C.G.R. group round robin test material (A533 B Cl 1). The specimens were tested in P.W.R. environments (288 °C, $O_2$ <100 ppb) high purity water. Testing was conducted at 1 cpm and R-ratio of 0.2, sinusoidal waveform. The cyclic crack growth rates for two steels (A533B and a Cr-Mo-V steel) are shown in Fig. 2.19. The two steels were chosen since although they have the same sulphur content, there were marked differences in the MnS inclusion content, morphology and distribution.

The fractographic examination revealed principally three different fracture morphologies, Fig. 2.20.

(i) Transgranular, ductile striations, (ii) Transgranular 'brittle' striations, and (iii) Striationless cleavage-like fracture. A fairly dense aggregation of elongated MnS inclusions is evident whenever the fracture mode exhibits brittle features. Clusters of inclusions can generate a brittle mode of crack growth, which spreads like a fan over the remaining part of the fracture surface. This was evident only in A533B steel. In the Cr-Mo-V steel speci-

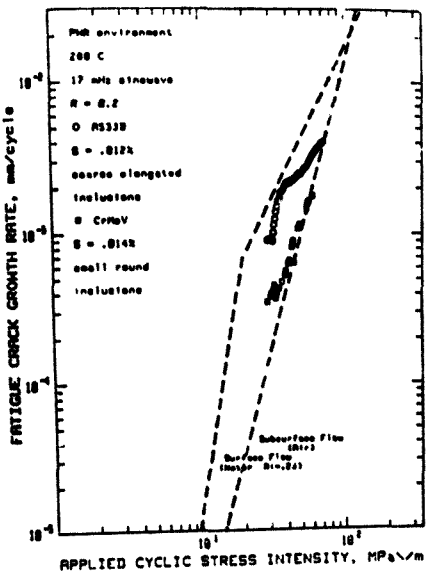


FIGURE 2.19: Test results of specimens selected for detailed fractographic evaluation: A533B steel (1HT14) and a Cr-Mo-V steel. Important test parameters are given in the da/dN - ΔK plot.

men, no similar fan shaped areas could be observed. This is probably due to the fact that in this steel the inclusions are small, round and more evenly distributed.

The inclusions are dissolved during the testing leaving only empty sites. However, near the crack tip partly dissolved MnS inclusions can be observed and next to the crack tip unchanged, exposed inclusions are present. Thus, the dissolution of MnS inclusions is a time dependent process. Hänninen et al. [38] favour hydrogen embrittlement as the main crack propagation mechanism (c.f. dissolu-

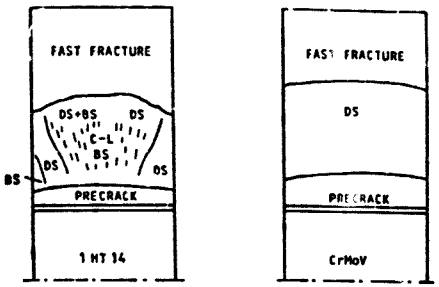


FIGURE 2.20: Schematic illustration of the macroscopic features of the fracture surfaces of A533B steel (1HT14) and Cr-Mo-V steel specimens. DS = ductile striations, BS = brittle striations, C-L = cleavage-like, elongated dots = inclusions.

tion controlled cracking). Their opinion is based primarily on the fractographic evidence discussed above. The above study shows that the MnS inclusion form, size and distribution has a more important impact on the fracture than the S content as such. Often inclusions are equated with cracks in the material. The beneficial aspect of spherical inclusions is in the reduction of notch sensitivity.

In Suzuki's study on SA533B Class 1 steel [39], major emphasis was placed on the crack growth along the weld heat affected zone. Effects of stress, waveform and hold time on the base material were also examined in connection with the possibility of time dependent cracking under sustained tensile stresses. The study revealed the following:

1. Triangular wave form resulted in an increase in F.C.G.R. with decreasing frequency (B.W.R. environment). All data followed a Paris type law and Table 2.5 gives the value of the exponent n.

TABLE 2.5

| Structure | Testing Environment | n |
|---|---|---|
| Base Metal | Water | 8 |
| | Air | 4 |
| HAZ (coarse grained martensitic) | Water | 5; 15 |
| | Air | 2.5 |
| HAZ (fine grained sorbitic) | Water | 3.4 |
| | Air | 2.5 |

2. In contrast to air testing it was found that microstructure had a large influence on fatigue crack extension in B.W.R. environment testing. The fine grained structure has a faster crack growth rate in the lower range of $\Delta K$, while the coarse grained structure has a faster crack growth rate in the upper $\Delta K$ range. Attention, therefore, should be devoted to the microstructural aspect to understand the crack growth characteristics of pressure vessel grade materials including weldments. The microstructural effect is more pronounced at higher temperatures.

James [40] undertook a number of experiments dealing with fatigue crack propagation in irradiated reactor pressure vessel steels, tested in air. The steels included ASTM alloys A302B, A533B, A508-2, A543 and weldments in A543 steel. Neutron implanted fluences and irradiation conditions were generally typical of those experienced by most power reactors. Neutron irradiation can produce significant changes in some of the properties of ferritic pressure vessel steels. It was therefore postulated that neutron irradiation should have a marked effect on the fatigue life of P.W.R. vessel steels, since fracture toughness behaviour is closely related to the concept of fatigue crack growth (the fracture toughness providing the 'end of life' criteria for terminating fatigue crack growth calculations). The study concluded that all data indicates that, under the conditions studied at 288 °C, neutron irradiation has a negligible effect upon the fatigue crack growth behaviour in the steels.

Cullen [41] also studied the effects of neutron irradiation and temperature on the F.C.G.R. of A508-2 steel, the main difference being that testing was carried out in a P.W.R. environment. Neutron irradiation was once again seen to have no effect on the F.C.G.R. of A508-2 steel. The effect of temperature was that the maximum F.C.G.R. occurred at about 200 °C for P.W.R. environment testing. For B.W.R. environment testing the opposite was found i.e., the minimum F.C.G.R. occurs at approximately 200 °C.

Corrosion fatigue of ASTM A302B steel in B.W.R. environments was investigated by Kondo et al. [42]. The results plotted as da/dN versus $\Delta K_I$, the stress intensity factor range, are shown in Fig. 2.21. The results indicate that the slope of in-air tests is 4, while those in high temperature water show the value 8 to 9.

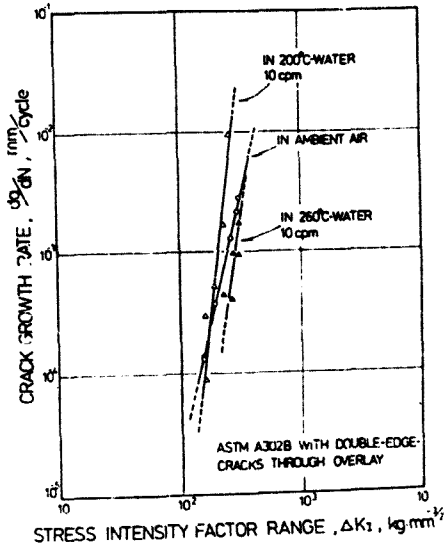


FIGURE 2.21: Effect of stress intensity factor on the crack growth rate [42].

The effect of temperature was seen to reverse at about 200 °C. Consequently, the fatigue crack growth seems to become moderate as temperature is shifted to that normally attained for power reactor operation. Frequency effects (see Fig. 2.22) show that the number of cycles to failure is steadily decreased as the frequency is decreased.

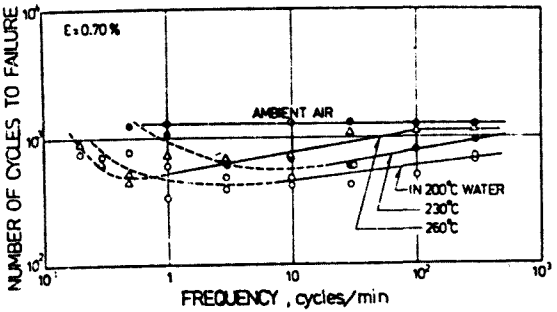


FIGURE 2.22: Plots of number of cycles to fracture as a function of loading frequency for fatigue testing in ambient air and in water [42].

However, below about 1 cpm, the F.C.G.R. tended to increase in a somewhat random fashion. Sometimes an incubation period was observed so that the life was extended.

### 2.3.2 Stress Corrosion Cracking

Clearly aspects of stress corrosion cracking (S.C.C.) are directly relevant to corrosion fatigue studies and hence it is desirable to have a full understanding of S.C.C. in carbon steels. The stress corrosion susceptibility of SA333 - grade 6 carbon steel was investigated over a broad range of temperatures in pure water containing controlled amounts of oxygen [43]. Experiments were conducted in high temperature/high pressure systems using slow strain rate tests (S.S.R.T.). The corrosion potential was measured and the potential plotted against dissolved oxygen.

The extremely large difference in potential for low and high values of dissolved oxygen (Fig. 2.23) cannot be explained by local corrosion rate effects or by thermodynamic explanations. A reasonable explanation for the large potential shift has been proposed for similar results with type 304 stainless steel [44]. In general, the carbon steel surface potential is dominated by exchange reactions of the metal surface with the dissolved gases, or the cathodic rather than anodic portion of the corrosion reaction (a system under cathodic control).

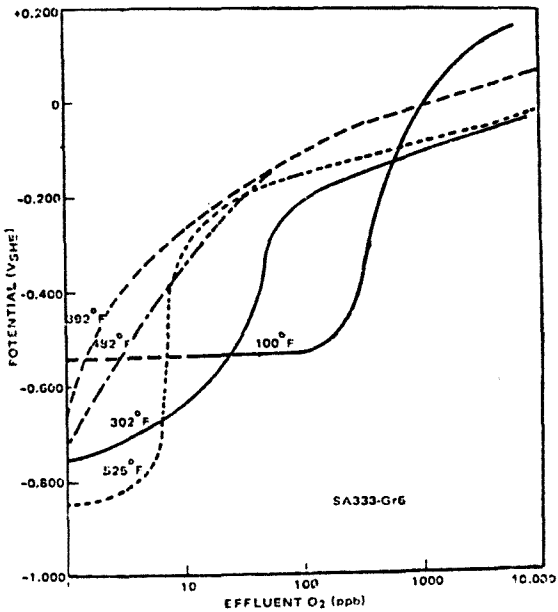


FIGURE 2.23: Potential/Oxygen summary [43].

At very low levels of dissolved oxygen, it is postulated that the dominant cathodic process is the reduction of protons to form hydrogen. Thus the carbon steel behaves like a hydrogen electrode. At the high oxygen concentrations, the cathodic process is undoubtedly the reduction of oxygen. The steep rise in the potential/oxygen curve results from a transition between the two reactions. The thermodynamic difference in potential between the two reduction reactions:

$2e + 2H_2O \rightarrow 2OH^- + H_2$ and

$4e + O_2 + 4H^+ \rightarrow 2H_2O$ is in good agreement with the experimental potential difference of 0.8 V at 525 °F.

Comparisons with even sensitized Type 304 stainless steel indicate that stress corrosion is generally a more difficult process in carbon steel. In high temperature water, it was found that the lower the potential, the less the susceptibility of Type-304 stainless steel to transgranular stress corrosion cracking [44]. Since, at any temperature it may be postulated that the lower the potential, the less susceptibility to stress corrosion. It may be predicted that from an environmental/electrochemical view, carbon steel ought to be more resistant to stress corrosion than stainless steel.

Stress corrosion cracking is known to be very specific in terms of material/stress/water chemistry combinations. Westinghouse data [15] shows that crack growth can be produced, particularly in HAZs of SA533B and SA508 material. However, the initial delay and subsequent intermittent nature of the cracking suggests that the conditions necessary to sustain stress corrosion cracking were not always present. It was concluded that static stress corrosion would be unlikely in a P.W.R. constructed of current materials with well controlled water chemistry. Furthermore, it should be noted that a breach of the cladding over the base metal defect is a necessary precursor for stress corrosion.

### 2.3.3 Fracture of the Cladding

Previously cracks in the ferritic body of the pressure vessel itself and their implications for its integrity under various condi-

tions have been considered. Although not directly vital to this question, the possible failure of the cladding is a matter of practical importance following the incidence of underclad cracking found in some vessels in France [45]. Underclad cracks resulting from the weld overlay process were usually rather small: up to a maximum of 7 - 8 mm high and 12 - 20 mm long in the direction perpendicular to the weld run. Considerations of cladding integrity are relevant to whether it is appropriate to use 'wet' or 'dry' conditions to assess the fatigue crack growth in the ferritic-base material. In principle, cracks could penetrate the cladding in three ways:

- by fatigue growth of either underclad cracks formed after the application of the stainless steel overlay or a pre-existing surface crack in the vessel wall;
- by the rapid extension out through the cladding of a crack in the vessel itself as a result of the high stress or strain developed in the ligament during a severe transient;
- by environmental cracking of the cladding itself.

Framatome have recently collated 60 sets of crack growth data for austenitic steels in the as-cast, wrought and welded condition, in air in the temperature range 260 to 320 °C at R-ratios ≤0.05 [45]. The data (Fig. 2.24) originated from Westinghouse, Hanford, General Electric, NRL and Creusot-Loire. Framatome fitted a curve of the form $da/dN = C\Delta K^4$ to the data from each test specimen, adjusting the value of C to ensure an upper bound to the crack length 'a' versus cycles 'N' curve. From this they obtained a crack growth equation which, when integrated, predicted the shortest life in this low R-ratio data as follows:

$$\frac{da}{dN} = 7.5 \times 10^{-13} \Delta K^4 \text{ metres/cycle } (\Delta K \text{ in MPa} \sqrt{m}) \qquad (2.8)$$

Experimental measurements of the growth of underclad cracks in clad specimens have also been made which indicate that the ra of

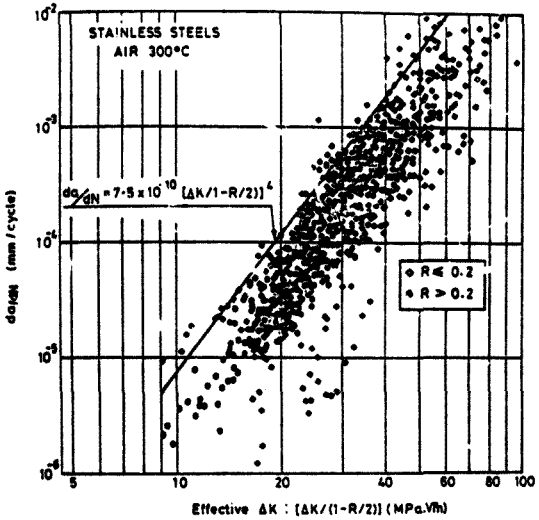


FIGURE 2.24: Compilation of crack growth rate data in the reduced form da/dN - $[\Delta K/(1-R/2)]$ for stainless steels in the 300 °C temperature range [45].

growth is the same as in specimens made solely of the cladding material [45].

The Framatome analysis [45] considered all normal and upset transients and indicated that for the inlet nozzle the maximum crack growth into the cladding from a crack 8 mm high initially would be 4.2 mm leaving a remaining minimum cladding ligament of 3.3 mm. The equivalent figures for the outlet nozzle are a crack growth of 4.0 mm and a remaining minimum cladding ligament of 3.5 mm. The actual clad thickness in these cases was 7.5 mm.

Type 304 and type 316 stainless steels have been examined in corrosion fatigue experiments in at least two laboratories, Westinghouse and Framatome. Results for simulated P.W.R. environments cover a range of frequencies from 1 Hz to $10^{-3}$ Hz and R-ratios from 0.2 to 0.7 [46, 47]. No significant effect of the P.W.R. environment on fatigue crack propagation in these steels was observed. Tests at high R-ratio (0.7) on aged (3000 hours at 427 °C) material showed an initial transient above this curve but the sustained growth rate is consistent with that obtained on un-aged material.

## 2.4 INTERPRETATION AND APPLICATION OF CORROSION FATIGUE CRACK GROWTH TO THE INTEGRITY OF P.W.R.'s

The following model has been put forward to explain Westinghouse results [15]:

It has been possible to examine the bounding rate of crack advance by electrochemical penetration alone and compare it with the mechanical fatigue crack growth rates for cycling over a range of frequencies. Important parameters are clearly a lower limiting value of $K_I$ denoting a given crack tip opening, $\delta$, which allows the exposure of fresh surface by oxide film rupture and transport of ions from the crack tip, and the rate of change of $K_I$, $\dot{K}_I$ or the strain rate $\dot{\varepsilon}$, which determines the rate of oxide fracture and repassivation. Qualitatively, the mechanistic picture once $K_I$ exceeds its limiting value, is that illustrated in Fig. 2.25. At very high frequencies the mechanical damage due to fatigue cycling occurs at such a rate that no electrochemical process can produce damage at a comparable rate. At intermediate frequencies, the oxide can be ruptured at a rate which allows significant electrochemical activity which is comparable with, or greatly exceeds, the fatigue crack growth rate. Finally at very low frequencies the oxide rupture rate is so slow that repassivation occurs so rapidly compared with the mechanical fatigue damage component that again the electrochemical contribution is negligible. Thus a mechanism can be perceived for which, given any set of electrochemical conditions, there is likely to be a set of mechanical values, stress intensity range, R-ratio and frequency, which can maximise the electrochemical contribution.

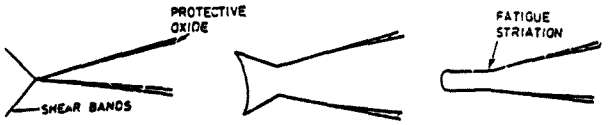


CASE (i) HIGH FREQUENCY: PROTECTIVE OXIDE FORMATION AND DISSOLUTION RATES TOO SLOW TO BE IMPORTANT COMPARED TO THE RATE OF FATIGUE DAMAGE.

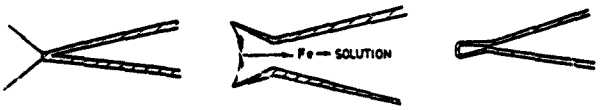


CASE (ii) INTERMEDIATE FREQUENCY: DISSOLUTION RATE COMPARABLE WITH OR GREATER THAN FATIGUE DAMAGE RATE BUT REPASSIVATION TOO SLOW TO PREVENT SIGNIFICANT ELECTROCHEMICAL ACTIVITY COMPARED TO THE FATIGUE DAMAGE

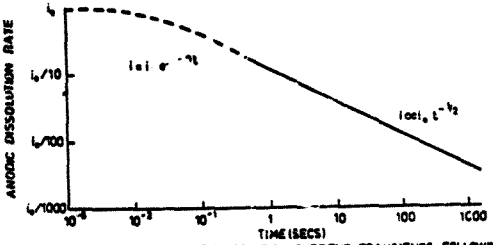


DIAGRAMMATIC REPRESENTATION OF DISSOLUTION CURRENT TRANSIENTS FOLLOWING OXIDE RUPTURE

CASE (iii) LOW FREQUENCY: ALL SURFACES PROTECTED BY AN OXIDE FILM AT 'ALL TIMES' RELATIVE TO THE RATE OF MECHANICAL FORMATION. IN SOME CIRCUMSTANCES THE OXIDE CAN ARREST FATIGUE CRACK GROWTH COMPLETELY AT VALUES OF $\Delta K$ WELL ABOVE THOSE ASSOCIATED WITH THE IN-AIR FATIGUE CRACK GROWTH THRESHOLD.

FIGURE 2.25: An illustration of the competition between oxide rupture, passivation and mechanical) fatigue damage in a material-environment combination which exhibits passivity [15].

The uses of fatigue crack growth analysis are many and varied, but the primary purpose of such an analysis from the standpoint of Section XI of the ASME Code is to estimate the growth which a flaw detected during inspection would experience during an upcoming period of service. This calculation is part of the process of determining whether the detected flaw should be repaired, or whether the size of flaw, even after its expected growth, is still small enough to leave the integrity of the structure unaffected.

Appendix A of Section XI to the ASME Code has shown good reliability for air tests. However the reference curve for water environment was based on very little data, and recent results have shown that the actual behaviour is considerably different. In a water environment, the crack growth is strongly affected by the R ratio (minimum load/maximum load) in addition to the range of applied stress intensity factor. Also the shape of the crack growth behaviour is not a single straight line, as presently shown on a logarithmic scale, but is curved, with the slope of the growth rate curve somewhat lower at high values of applied stress intensity factor as shown in Fig. 2.26 [48]. Thus revision of this reference curve was reconsidered.

It is important to reach some overall conclusions concerning the crack growth rate behaviour of the steels of interest in light water reactor environments (same trends expected in P.W.R. environments). To this end Fig. 2.27 was prepared. Although it is schematic in nature, it is helpful in conveying certain trends and is believed to be rather close to the true behaviour. At low $\Delta K$ values the crack growth rate is not accelerated and is the same as in air. As $\Delta K$ increases, the crack growth rate increases dramatically. The point at which the crack growth accelerates is dependent on the R ratio, as shown in the figure. At higher R ratios the growth rate takes off sooner, but this effect is believed to saturate at R equal to about 0.70 - 0.75. The amount of acceleration is dependent on the cyclic frequency or loading rate of the test, with the most acceleration at lower frequencies or equivalently slower loading rates. This effect is also believed to saturate at 0.1 to 1.0

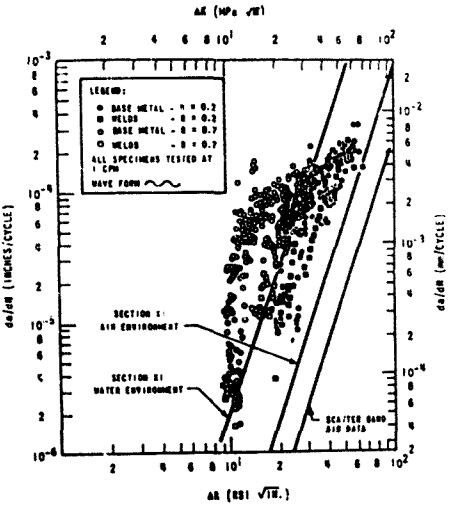


FIGURE 2.26: Effect of R ratio - 533BCA-1 and 508CA-2 base metal and welds in P.W.R. environment [48].

cycle per minute. As shown in the figure, the crack growth rate increases more slowly with ΔK once the plateau is reached, and eventually rejoins the air crack growth curve.

## 2.5 PROGRESS IN FATIGUE CRACK GROWTH RATE DATA ACCUMULATION

Within the last few years, several other laboratories have commissioned experimental rigs for corrosion fatigue studies in L.W.R. environments. Figure 2.28 shows some recent results obtained for the U.K.A.E.A. P.W.R. project for SA-533B steel in P.W.R. water of various compositions at 288 °C [49]. A comparison with Fig. 2.11 reveals that there was comparatively little effect of these aqueous environments on crack growth for cyclic frequencies in the range 10 to 0.0167 Hz compared with tests carried out in helium gas at the

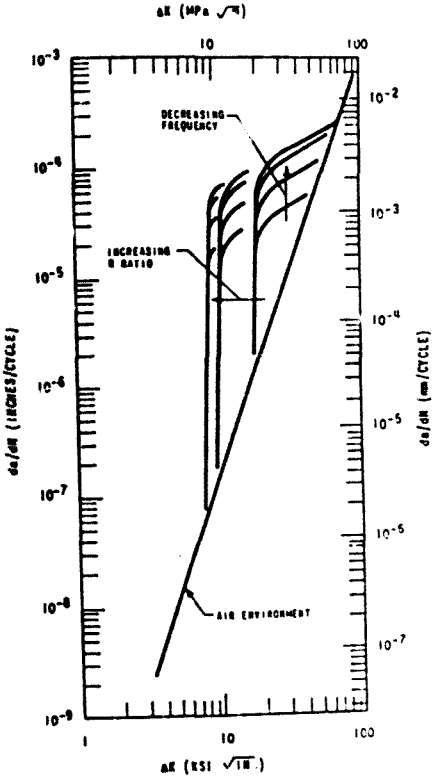


FIGURE 2.27: Schematic of frequency and R ratio effects - pressure vessel steels in L.W.R. environment [48].

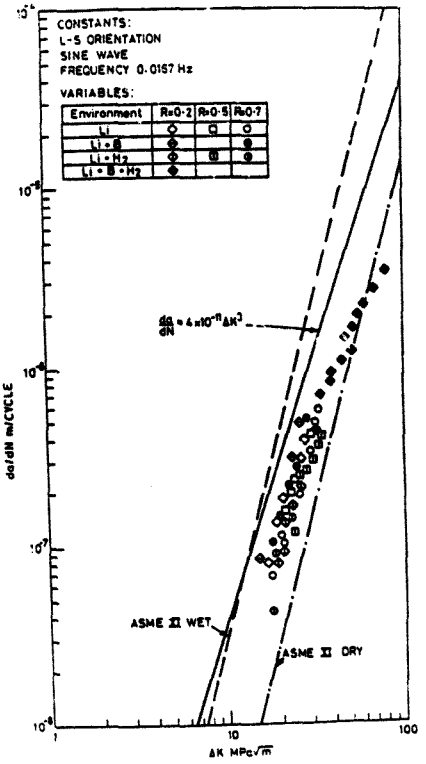


FIGURE 2.28: U.K.A.E.A. crack propagation data for A533-B steel in P.W.R. primary water of various compositions at 288 °C [49].

same temperature. An upper bound to these results representing an increase in growth rates of no more than four times those observed in an inert environment is:

$$\frac{da}{dN} = 4 \times 10^{-11} \Delta K^3 \text{ metres/cycle } (\Delta K \text{ in MPa } \sqrt{m}) \qquad (2.9)$$

Their data at room temperature [53] has not shown an increase in growth rate compared with that obtained at 300 °C. This increases confidence in using the same crack growth equations for evaluating plant transients which involve cooling to low temperatures as well as those occurring primarily around 300 °C. However, the influence of temperature on corrosion fatigue crack growth is not well characterized over the whole temperature range and some experimental work devoted to this aspect is required.

An examination of the Westinghouse data has revealed that the older and more impure steels containing >0.015% sulphur gave high crack propagation rates, whereas low sulphur steels <0.010% exhibited smaller environmental enhancement factors [52]. This conclusion specifically referred to experiments at relatively low R ratios of ~0.2. Framatome has also reported results which support the conclusion regarding the importance of steel sulphur content under similar test conditions. Westinghouse have recently tested examples of the U.K.A.E.A SA5338 plate specimens at a high R ratio of ~0.7 and preliminary analysis shows high crack growth rates comparable with much of their experimental data to date.

It has become apparent from a round robin test series that water flowrate past the specimens could be an important factor. Only very low flowrates - static systems, were used in both the Westinghouse and Framatome experiments, whereas a flowrate designed to give turbulent flow past the specimens was used in the U.K.A.E.A. programme. Turbulent flow conditions are relevant to most locations of the pressure vessel in an operating plant, the excention being the upper head area.

Variability in data from different experimental rigs on nominally the same materials is strong circumstantial evidence that particular metallurgical and water conditions combine to produce the electrochemical conditions (i.e. the electrochemical potential) necessary for high sustained environmental cracking rates. However, the evidence suggests that clean, low sulphur steels combined with realistic turbulent flowrates lead to lower crack growth rates.

Further evidence for the importance of the electrochemical potential which is established by steel in simulated water reactor coolants comes from investigations using B.W.R. water at 288 °C and steels to the same or similar specifications as for the P.W.R. programme. Very small concentrations of oxygen of the order of 10 - 100 ppb can produce step changes in potential which are flowrate dependent. At very high oxygen contents of the order of 8000 ppb (air saturation at room temperature), corrosion fatigue and constant extension rate tests at 288 °C indicate considerable environmental cracking sensitivity and high rates of crack growth. In particular the constant extension rate test results for stress corrosion cracking are known to be flowrate, oxygen concentration and temperature dependent, all indicative of a strong dependence on electrochemical potential established under each environmental condition. These B.W.R. results as they stand may not be strictly relevant to the P.W.R. case except possibly under start-up conditions but they do emphasize the important rôle of oxygen at extremely low concentrations and by implication, potential, in experimental work in this area.

No studies of the influence of irradiation simultaneous with corrosion on environmental crack growth have been published for pressure vessel steels. However, results on steel pre-irradiated to typical end-of-reactor life, doses of $5 \times 10^{19}$ neutrons/cm$^2$ ($E > 1$ MeV), have shown no additional effect on crack growth rate. The effect of ionizing radiations on the oxidizing potential of the environment could possibly influence environmental crack growth, although the probability is not considered to be high in the chemically re-

ducing P.W.R. water environment, certainly at temperatures >80 °C where ionizing radiations initiate a rapid reaction between molecular hydrogen and oxygen.

Defect-free cladding constitutes a significant barrier against the ingress of water to any cracks beneath the cladding. Under these circumstances the dry crack growth equations would apply. However, in the unlikely situation that water ingress to a sub-cladding crack occurs, then the calculations of crack growth must be based on corrosion fatigue and stress corrosion data:

a) The data base for corrosion fatigue crack growth in pressure vessel steels exposed to P.W.R. water has increased substantially over the past decade. In spite of this, significant variations in the results from individual laboratories still exist and the available data relates directly to only a limited range of the transients experienced by a P.W.R. pressure vessel.

b) Only limited data is available on relevant materials (little for weldments) in high flowrate P.W.R. primary water. These show significantly lower growth rates than the bulk of the Westinghouse data which were obtained mainly on high sulphur steels in low flowrate conditions. Modern steels in well controlled normal flowrate P.W.R. primary water are not expected to give rates of corrosion fatigue crack growth more than four times greater than those obtained in an inert environment at the same temperature. However, because of the limitations in material variables covered in the U.K.A.E.A. experiments, the Westinghouse data base cannot at this time be disregarded as irrelevant to a U.K. P.W.R.

c) A mechanistic interpretation of the corrosion fatigue data has been developed. It is based on a working hypothesis that high corrosion fatigue crack growth rates arise only when a strain rate sensitive stress corrosion process under crack tip dissolution rate control operates coincidentally with fatigue crack growth. Most transient events on a P.W.R. would lead to strain

rates below the effective strain rate threshold. Nevertheless, further work is required to validate this mechanistic interpretation and it would appear that hydrogen embrittlement processes can be easily applied to explain large increases in crack growth rates and many microstructural features.

d) The Westinghouse corrosion fatigue data forms the basis of the growth rate equations given in the recent revision of ASME Section XI, Appendix A (1980). It is predicted that a crack in the bottom head 37.5 mm high initially would grow a maximum of 28 mm during one design life. Similarly a line crack initially 25 mm high would grow a maximum of 7 mm. The higher growth rates represented by the Code are unlikely to occur in practice and therefore calculations based on it would be conservative. Careful attention will need to be given to sulphide inclusion, size, shape and morphology characterization.

## 2.6 SUMMARY

The fatigue properties of a P.W.R. are influenced by the P.W.R. environment resulting in a synergistic action of a corrosive environment and fatigue.

There appear to be two main 'schools of thought' concerning mechanisms of C.F. crack growth. Firstly localized plastic deformation arising from cyclic loading causes the disruption of otherwise protective surface films and hence promotes electrochemical activity. Secondly, hydrogen embrittlement processes causing regions of fast fracture especially about MnS inclusions. The latter model is gaining more and more credibility as a result of microstructural observations, but clearly both crack growth mechanisms could be resulting in accelerated C.F. crack growth.

Fatigue crack propagation in air in SA533B and SA508 steels and typical weldments is comparatively well categorized. The range of variables covers frequencies from 0.017 to 60 Hz, temperatures from 20 to 300 °C, specimen thickness from 5 to 100 mm, stress ratio

from 0 to 0.8 and neutron irradiation up to total doses of 5.7 x $10^{19}$ neutrons/$cm^2$. None of these variables has significantly increased or decreased crack growth rates outside the scatter band observed in room temperature air and whose upper bound is represented by the 'High R Dry' curve in the ASME XI Code specification. This may, however, not be the case when embrittled or segregated crack growth pathways exist.

Data produced by Westinghouse for P.W.R. environment testing has shown results to be consistent with the new ASME XI Code for high R ratio testing. Fracture surfaces have shown ductile striated growth. However, brittle cleavage facets have been observed in SA533B steel [26] and crack growth rates have been shown to be larger than those predicted by the old 'ASME XI WET' curve (1974).

To date, some of the testing variables that have been investigated include different parameters on metallurgical, mechanical and chemical factors. Amzallag et al. [27, 28] have shown that high sulphur steels exhibit faster crack growth rates than low sulphur steels. Clearly this effect will depend on sulphide size, shape and morphology. The work also revealed that sinusoidal waveform loading is the most detrimental. This has been confirmed by other authors [29, 30] who have investigated sinusoidal, triangular, sawtooth and trapezoidal wave loading. Amzallag's work showed little effect of R-ratio on the crack growth rates of low sulphur A533-B-1 steel. Testing at various frequencies (0.1 cpm to 5 Hz) did not show a significant increase in crack growth rates for very low frequencies. Metallurgical examinations have revealed that fast crack growth rates correspond to brittle fractographic features and local brittle features occurred about MnS inclusions. Low crack growth rates, which correspond closely to air line data show ductile (striated) fracture surfaces.

Scott's work [34] has placed an emphasis on metallurgical aspects (different heats) on crack growth rates of A533-B steel in P.W.R. primary water at 288 $^{o}$C using a fast flowrate test rig. Steel samples were interchanged between laboratories (Harwell and

Westinghouse) and results varied by up to 10 times. It was therefore postulated that differences in results were probably not due to MnS stringer effects. Clearly this would depend on MnS stringer's size, shape and morphology about the crack plain. Scott explained the results by stating that electrochemical conditions within different rigs might be different.

Atkinson [36] concluded from his studies on A533-B-1 steel that crack growth rates increase with decreasing frequency but that the effect only lasts until some 'peak' frequency is reached after which crack growth rates decrease with decreasing frequency. F.C.G.R.'s all increased with increasing test temperature in the range 20 - 90 °C.

Hänninen [38] has presented voluminous work whereby his experimental data is explained using a hydrogen-induced cracking model. Two steels of similar composition, but marked differences in sulphide size, shape and morphology were tested in P.W.R. environments. Brittle fan shaped fractographic features about MnS inclusions led to increased crack growth rates. Spherical inclusions were shown to have a beneficial effect since they reduce notch sensitivity.

Suzuki's work [39] on SA533B Cl1 heat-affected zone testing showed a large microstructural effect in B.W.R. environments which increases with temperature. All tests did therefore not show enhanced crack growth rates with respect to the base plate.

James' studies [40] revealed that for air tests, neutron irradiation had little effect on the fatigue crack growth rates of pressure vessel steels. Cullen [41] has since carried out similar experiments in P.W.R. water and he also found little effect of neutron irradiation. Cullen also showed that in P.W.R. environments a temperature of 200 °C gave the highest crack growth rates for R.P.V. steels (the opposite was true for B.W.R. environments). This observation was confirmed by Kondo [42] for A302B steel in B.W.R. environment testing.

Framatome have recently collated 62 sets of crack growth rate data for austenitic cladding steels. The analysis that followed showed that during a typical 'life-time' pre-existing cracks of assumed proportions would not grow through the cladding.

The production of voluminous data will eventually lead to a clearer understanding of F.C.G.R.'s in P.W.R. environments. However, careful attention must be given to testing conditions, specimen characterization and data interpretation.

## 3.0 DESIGN OF WATER CONDITIONING AND CORROSION FATIGUE TESTING LOOPS

The water chemistry make-up and flow system for the simulation of P.W.R. conditions has been designed from knowledge gained both through literature on the topic, as well as through discussions with several members of the I.C.C.G.R. group who are presently undertaking research in the field of corrosion fatique. Clearly the design has been modified in order to suit firstly the budget and secondly the local market i.e. all parts of the design are locally available or can be made locally. The initial design is for so-called 'low' temperature (room temperature to below the boiling point of water) and low pressure (close to atmospheric pressure) corrosion fatigue testing in simulated P.W.R. environments. However, flexibility needed to be incorporated into the design so that a high temperature (up to 300 °C) and high pressure (up to 14.5 MPa) corrosion fatigue facility could, in due course, be linked to the water chemistry make-up and storage facilities. The facility for carrying out both low temperature (T), pressure (P) and high T, P tests simultaneously was deemed necessary.

Figure 3.1 is a flow diagram of the low T, P loop and water conditioning unit. This set-up is envisaged for dual testing conditions (i.e. low T, P and high T, P testing). The high T, P loop can simply be coupled (via Swagelok fittings) to the 450 ℓ supply tank.

Tap water is processed by filtration and deionization before being treated in an activated carbon-virgin resin bed, oxygen scavenger bed, and a final polishing unit. The demineralized, deoxygenated water is then passed through a fine filter before entering either the make-up or storage tanks. The conditioned water will be stored in a storage tank of about 450 ℓ capacity. This tank will serve as a 'base' for recirculating water, since the unit will need to be run as a recirculating system. This is necessary for a number of reasons. Firstly the deionizer capacity will not be able to cope with long periods of use without regular replacement of the cartridges. Secondly, dosing chemicals will be lost to the drain, and

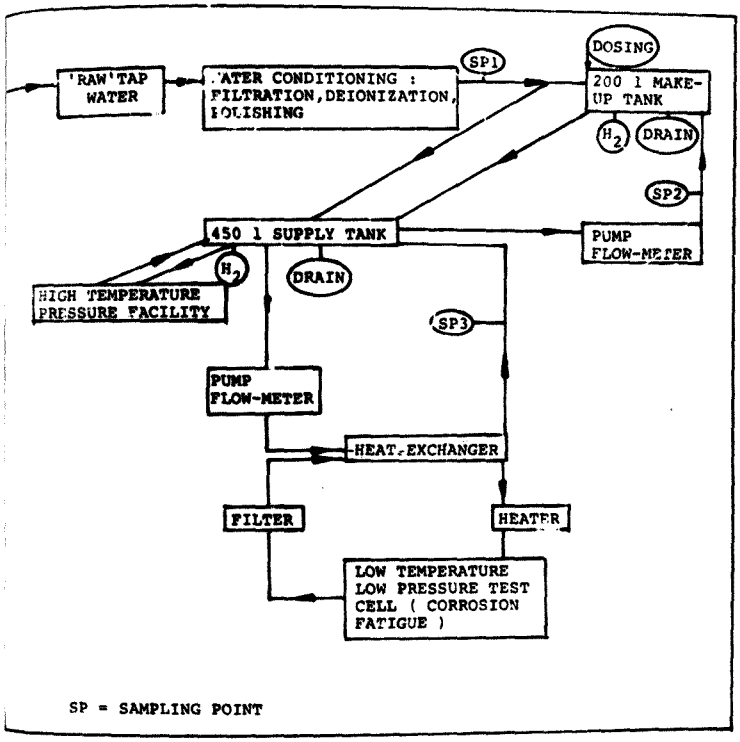


FIGURE 3.1: Flow diagram of the water conditioning, low temperature - low pressure loop with high temperature - high pressure loop facility.

this is simply uneconomical. Thirdly, water conservation is imperative in the Republic of South Africa. The economics of the situation dictate that a recirculating system without water clean-up (following the initial clean-up process) should be carried out. When water chemistry levels are not to specification, the stored water will need to be discarded and a new batch will need to be made-up.

Both the 200 ℓ make-up tank and the 450 ℓ storage tank have hydrogen gas bubbling facilities. This means that oxygen levels can be reduced by purging with hydrogen and the water will therefore be kept under a hydrogen blanket. Continuous venting to atmosphere can be obtained through pressure relief valves, although this might not be necessary once oxygen levels are within specification.

Both tanks have a hexagonal bolt on the tank roof. However, once these bolts are removed for dosing to take place, oxygen will flow into the system. Dosing (boric acid, lithium hydroxide) will therefore need to be carried out in the 200 ℓ make-up tank, which can be isolated by valves from the rest of the system.

Once dosing is complete, hydrogen purging can be used to reduce oxygen levels to those of the 450 ℓ storage tank. Both tanks can then be pump mixed using polyethylene diaphragm pumps.

As the high T, P corrosion fatigue facility will only be introduced at a later stage it will not be discussed in this thesis. Only low T, P testing will be carried out and it was therefore found that the 450 ℓ tank need not be incorporated into the testing loop. Figure 3.2 shows the modified flow chart for the low T, P testing facility. The use of the 200 ℓ tank has made testing more economical in that: (1) The amount of make-up water required is reduced; (2) The time to reduce oxygen levels is lowered and therefore less hydrogen is consumed; (3) The quantity of chemicals required for dosing will also be reduced. The 'problem' of allowing oxygen ingress to the system during dosing is minimized by the relatively short time required to reduce the oxygen levels during hydrogen bubbling.

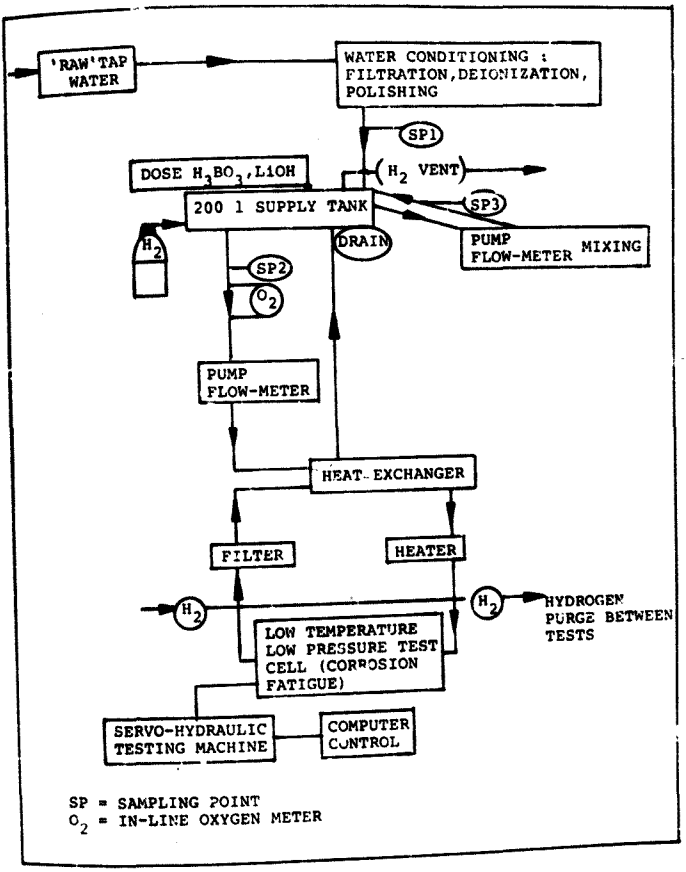


FIGURE 3.2: Revision of flow diagram for low temperature - low pressure loop.

The system has been piped using low density polyethylene (L.D.P.E.) tubing and all valves and relating couplings have been manufactured from brass or cadmium coated brass. Such fittings are used extensively in the petrochemical industry. The use of plastic tubing and brass fittings was chosen because of the economics. Economic considerations preclude the use of stainless steel valves and fittings. It was also thought to be a good trouble shooting exercise in that experimentation with the flow loop system could be carried out relatively easily. Budget requirements meant that L.D.P.E. pump heads were required instead of stainless steel and therefore the use of L.D.P.E. tubing was justified.

Analytical chemistry facilities would be needed to determine: Boron, Lithium, Chloride, Fluoride, pH, Conductivity, Oxygen, Hydrogen and Sulphate concentrations.

## 3.1 WATER CONDITIONING

Tap water is initially passed through a Sartobran Capsule filter. A similar design filter is placed after the corrosion fatigue testing cell so that contaminated water is filtered before entry into the storage tank. These filters are complete filter units for reliable and economic filtration. The Sartobran Capsule filters are presterilized with ethylene oxide gas and can be repeatedly autoclaved at 121 °C in which gas and chemical sterilization are also possible. Subsequently, after connection of the tubing, the filtration system is ready for use. These complete units are both disposable and reusable, and both cleaning and autoclaving are extremely simply. The main advantages of these filters are the small dimensions and the large filtration area.

The filters contain cellulose acetate filter material and are seated in polypropylene housings. The maximum operating pressure is 4 bar and operating temperatures of 120 °C. Connections are 10 mm house nipples and two screw-hole valves can be used for venting trapped gas.

The filter for tap water cleaning has a 3 μm absolute rating and is used to prolong the life of the deionization and deoxygenation plant. The filter positioned after the corrosion fatigue cell has a 0.2 μm absolute rating (i.e. 100% confidence that all material greater than 0.2 μm will not pass through the filter). The choice of 0.2 μm is consistent with the final filter after the water processing unit (0.2 μm Pall filter). This means that no material greater than 0.2 μm will be present in the storage tank water.

After the filtration pretreatment, the water passes through a 25 ℓ capacity mixed bed deionizer before entry into the main clean-up section. This rougher serves to increase the ion removal capacity at a later stage and, more importantly, helps to reduce replacement time on the final deionization cartridges. Thus the initial deionization column improves the running cost efficiency of the plant. (Plate 3.1 shows the filter and deionizer.)

PLATE 3.1: Filter (3 micron absolute rating) and 25 ℓ mixed bed deionizer.

The 'roughed' water then passes into a NANO pure II deionizer. The NANO pure system can deliver water with the following characteristics:

| | NANO pure II |
|---|---|
| Conductivity ($\mu s.cm^{-1}$ Min) | Down to 0.05 |
| Specific Resistance (Megohm, Min) | Up to 18.3 |
| Total Solid Matter (Mg/ℓ, Max) | <0.1 |
| Silicate (Mg/ℓ, Max) | <0.01 |
| Culture/Colony Count (Colony forming units/mℓ) | <10.0 |

The system measures up to the stringent requirements of: A.S.T.M., C.A.P. (College of American Pathologists); N.C.C.L.S. (National Committee for Clinical Laboratory Standards). i.e. producing type 1 grade water. Type 1 water will be free of particulate material larger than 0.2 μm. (Free of particulate matter is defined as less than 500 particles/ℓ which are greater than 0.2 μm.) (Plate 3.2 shows the NANO-pure II system.)

PLATE 3.2: NANO pure II water treatment facility

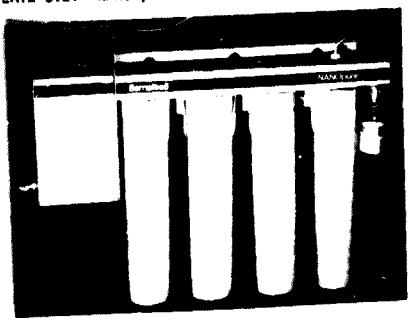

The NANO pure II (Fig. 3.3) incorporates a microprocessor-controlled purity system that automatically:

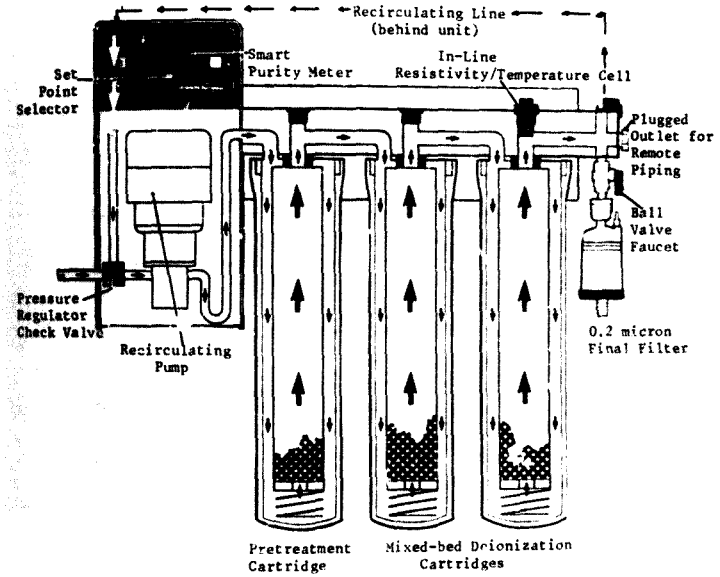


FIGURE 3.3: NANO pure II water purification unit

1. Monitors ion exchange cartridge conditions with a resistivity sensor that is mounted in-line as required by A.S.T.M. It compares purity against user selected limits of 16.7, 10 and 1 megohm - cm. If purity falls below the set point the system warns the operator with a blinking display.

2. Monitors the resistivity cell for low water levels, entrapped air or cell failure and alerts operator by a blank display and blinking decimal points.

3. Measures temperature with a R.T.D. (resistance thermometer device) which is superior to a conventional thermistor, and therefore gives more accurate resistivity measurements.

4. Temperature compensates resistivity readings to 25 °C as prescribed by established standards.

5. Checks digital display. All segments and decimals are illuminated when the system is turned on, for visual verification.

6. Performs a periodic check of the measurement circuit and alerts operator by displaying a 'C' if performance is not within tolerance limits, eliminating the need for a manual test button.

7. The temperature of the water within the system may be displayed with a simple push of a button.

The main advantage of the NANO pure II system is that it is extremely easy to maintain. Cartridges are simply unscrewed and replaced. The pump has an automatic switch-off device if inlet pressures become too high. (This prevents destruction of the system.) The unit can deliver a maximum flowrate of 120 ℓ/hr.

The NANO pure II system being used in the P.W.R. corrosion fatigue work contains four cartridges:

No. 1: Pretreatment cartridge: The cartridge increases the ion removal capability of standard mixed bed cartridges by a factor of 30. It contains a combination of granular activated carbon and virgin, macroreticular resin. It effectively removes colloids, bacteria, organics and chlorine. The bacteria removal capability in conjunction with the recirculation system of NANO pure II is particularly effective in maintaining low bacteria levels throughout the system, thus prolonging the 0.2 μm filter life.

**No. 2:** Oxygen removal cartridge: This cartridge is identical to cartridge No. 4, the only difference being that the ultra-pure cartridge has been regenerated with sodium metabi-sulphate. This bonds to the resin and acts as an oxygen scavenger by reducing $O_2$ levels from 8 ppm to less than 1 ppm. A product of the reaction is the formation of $SO_4^{2-}$ ions which need to be removed in cartridges No. 3 and No. 4.

**No. 3:** High capacity cartridge: The high capacity mixed bed deionizer cartridge is used as a 'rougher' in the 4-module units. It has more grain removal capacity than the ultra-pure cartridge, but to a lower purity level. When used in conjunction with the ultra-pure cartridge it dramatically prolongs their life and performance by a factor of 2 and cuts operating costs by as much as one third.

**No. 4:** Ultra-pure cartridge: The ultra-pure mixed bed deionization cartridge produces water with a resistivity up to 18.3 megohm-cm. Ultra-pure cartridges contain nuclear grade strong acid cation and strong base anion resins in a mixed bed form to achieve this high purity performance. It has a total grain removal capacity of about $^2/_3$ that of the 'rougher' cartridge but it is indispensable for the production of high purity water.

After the demineralized water has passed through the cartridges, it can be recirculated for further clean-up, or it can be passed through a final 0.2 μm filter (absolute rating) before being passed into the 200 ℓ tank (Fig. 3.2). The 0.2 μm filter is a pleated membrane filter that removes all bacteria. These filters are radiation sterilized at time of manufacture.

## 3.2 CORROSION FATIGUE TESTING LOOP

Following the production of demineralized water, the water flows into the 200 ℓ supply tank. At this point the water is dosed with boric acid and lithium hydroxide to simulate P.W.R. environment conditions (Plate 3.3 shows the supply tank). Hydrogen purging through the tank ensures that the oxygen levels are reduced to